NASA/CR-2001-211247

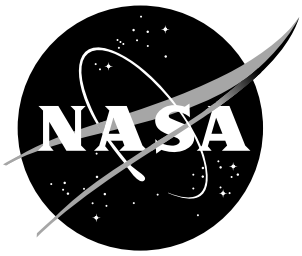

Structural Acoustic Prediction and Interior Noise Control Technology

G. P. Mathur, C. L. Chin, M. A. Simpson, and J. T. Lee
The Boeing Company, Long Beach, California

November 2001

The NASA STI Program Office ... in Profile

Since its founding, NASA has been dedicated to the advancement of aeronautics and space science. The NASA Scientific and Technical Information (STI) Program Office plays a key part in helping NASA maintain this important role.

The NASA STI Program Office is operated by Langley Research Center, the lead center for NASA's scientific and technical information. The NASA STI Program Office provides access to the NASA STI Database, the largest collection of aeronautical and space science STI in the world. The Program Office is also NASA's institutional mechanism for disseminating the results of its research and development activities. These results are published by NASA in the NASA STI Report Series, which includes the following report types:

- TECHNICAL PUBLICATION. Reports of completed research or a major significant phase of research that present the results of NASA programs and include extensive data or theoretical analysis. Includes compilations of significant scientific and technical data and information deemed to be of continuing reference value. NASA counterpart of peer-reviewed formal professional papers, but having less stringent limitations on manuscript length and extent of graphic presentations.

- TECHNICAL MEMORANDUM. Scientific and technical findings that are preliminary or of specialized interest, e.g., quick release reports, working papers, and bibliographies that contain minimal annotation. Does not contain extensive analysis.

- CONTRACTOR REPORT. Scientific and technical findings by NASA-sponsored contractors and grantees.

- CONFERENCE PUBLICATION. Collected papers from scientific and technical conferences, symposia, seminars, or other meetings sponsored or co-sponsored by NASA.

- SPECIAL PUBLICATION. Scientific, technical, or historical information from NASA programs, projects, and missions, often concerned with subjects having substantial public interest.

- TECHNICAL TRANSLATION. English-language translations of foreign scientific and technical material pertinent to NASA's mission.

Specialized services that complement the STI Program Office's diverse offerings include creating custom thesauri, building customized databases, organizing and publishing research results ... even providing videos.

For more information about the NASA STI Program Office, see the following:

- Access the NASA STI Program Home Page at ***http://www.sti.nasa.gov***

- E-mail your question via the Internet to help@sti.nasa.gov

- Fax your question to the NASA STI Help Desk at (301) 621-0134

- Phone the NASA STI Help Desk at (301) 621-0390

- Write to:
  NASA STI Help Desk
  NASA Center for AeroSpace Information
  7121 Standard Drive
  Hanover, MD 21076-1320

NASA/CR-2001-211247

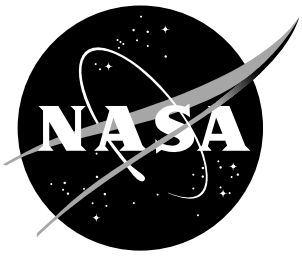

Structural Acoustic Prediction and Interior Noise Control Technology

G. P. Mathur, C. L. Chin, M. A. Simpson, and J. T. Lee
The Boeing Company, Long Beach, California

National Aeronautics and
Space Administration

Langley Research Center
Hampton, Virginia 23681-2199

Prepared for Langley Research Center
under Contract NAS1-97040

November 2001

Available from:

NASA Center for AeroSpace Information (CASI)
7121 Standard Drive
Hanover, MD 21076-1320
(301) 621-0390

National Technical Information Service (NTIS)
5285 Port Royal Road
Springfield, VA 22161-2171
(703) 605-6000

Preface

This report was prepared by Boeing Phantom Works - Long Beach under Task Assignment 14 of Contract NAS1-97040 with NASA Langley Research Center, Hampton, VA. The NASA technical monitor was Daniel L. Palumbo.

This report describes work performed during FY 2000-2001. Dr. Gopal P. Mathur was the principal investigator. Gopal Mathur and Cliff Chin prepared this report. Dr. Cliff Chin developed the 3-dimensional FE modeling and code of the poro-elastic foam coupled with vibrating structures. Cliff Chin also developed the FE models of the double wall system with foam for prediction of its TL. Joshua Lee developed the active control algorithms and implemented them within the FE code. Gopal Mathur coordinated the smart foam tests with the Virginia Tech team (Dr. Chris Fuller, Dr. Mike Kidner and Pierre Marcotte). The smart foam tests were conducted at the Boeing Noise Engineering Laboratories in Seattle, Washington with the support of Mr. Eric Hofbeck of the Noise Laboratories. Myles Simpson provided overall technical guidance on the project.

Table of Contents

List of Tables

List of Figures

1. INTRODUCTION

The overall objective of the Interior Noise Reduction subelement of NASA's Advanced Subsonic Technology program is to develop and validate weight-efficient technology to minimize cabin and cockpit noise in commercial and general aviation aircraft. The goal of this development and validation effort is to produce technology capable of yielding a 6 dB overall interior noise reduction by the year 2001.

To help achieve this goal, two subtasks were conducted by the Boeing Company in 2000-2001 under Task 14, “Structural Acoustic Prediction and Interior Noise Control Technology,” of Contract NAS1-97040. One of the subtask involved development of finite-element based prediction models and validation of the models with test data, while the other subtask involved development and laboratory testing of smart foam for noise control treatments.

The next section of this report describes the development of a finite-element code for modeling and determining response of vibrating structures lined with poroelastic foam. The FE model was used to predict the structural response and transmission loss of a double wall panel, simulating a structure with a trim panel, and treated with passive foam. Comparison of these predictions with the available data is used to validate the FE method.

Section 3 discusses the results of transmission loss tests with passive and combined passive/active treatments applied to a 757-sidewall test section. These treatments employ various designs using "smart foam" elements. Such elements combine acoustic foam for high frequency passive noise reduction with embedded active piezoelectric elements for low frequency noise control, and also include an additional distributed mass to provide tuning of the element to reduce noise in a specific frequency range.

In section 4, a smart foam configuration and overall system design that could be installed on NASA’s 757 experimental aircraft for flight-testing is presented. This proposed design is based upon the results of the 757-sidewall tests, combined with the results of earlier NASA-funded work performed at Virginia Tech in which multiple de-coupled control elements were used instead of a fully coupled system.

Section 5 summarizes the conclusions of all the subtasks, and provides recommendations based on the results. References are listed in Section 6.

The appendix contain a description of: (i) stiffness and mass matrices for FE modeling of poroelastic foam and acoustic media.

2. FINITE ELEMENT MODELING OF SMART FOAM SYSTEM FOR PASSIVE/ACTIVE NOISE CONTROL

2.1 INTRODUCTION

The smart foam noise control system is designed to reduce sound by a combination of the passive absorbing component of the poroelastic foam and the active component of the voltage-driven PVDF (polyvinylidene fluoride) film [1]. In general, the passive foam works well in middle to high frequencies while the active component provides cancellation for low frequencies. In combining active and passive concepts, a hybrid noise control methodology is obtained which allows the control of noise over a wide frequency bandwidth.

The purpose of developing this smart foam finite element model is to provide prediction capabilities for varied configurations ranging from a single medium, such as structure, air space, foam and PVDF film, to a system made of coupled multiple media, like the Distributed Active Vibration Absorber (DAVA) system as mentioned in [2]. In order to achieve this, a three-dimensional smart foam finite element model was developed to incorporate foam, acoustic, structural, mass and PVDF elements together to meet the diverse numerical simulations.

The three-dimensional model is based on a previously developed two-dimensional smart foam system. It has six additional types of elements in the three-dimensional (3-D) space (plate, beam, in-plane structure membrane, acoustic, poroelastic, and peizoelectric elements), plus their related coupling matrices for interfacing with the neighboring media. Except for the 3-D PVDF element and its coupling with poroelastic element, all other elements in the smart foam model have been validated against known data, as were their corresponding interface coupling matrices. Those verification cases are detailed in Section 2.5. Although the development of a 3-D PVDF element will be an ongoing task, the 2-D PVDF element was completely developed and incorporated with the poroelastic element from a previous work. Also, the feed forward open-loop control algorithm has been included to the 2-D smart system for implementing the active control under the current task, and some results will be discussed in a later section.

2.2 FINITE ELEMENT FORMULATIONS

The typical three-dimensional smart foam system without the PVDF film is depicted in Figure 2.1. The sound absorbing material, either fiberglass or acoustic foam, is inserted into an

air cavity which is enclosed by two elastic plates with arbitrary boundary conditions. The absorbing material could be bonded or unbonded to the plates. If it is unbonded to the plate, there will be a thin air gap between plate and the absorbing layer as shown in Figure 2.1. The double plate system is assumed mounted in a rigid baffle, and one plate is subject to acoustic excitation and another is radiating sound to the receiving room. Harmonic oscillation (e^{jwt}) is assumed for all excitation cases in this report.

2.2.1 Finite Element Formulation for Poroelastic Foam

Porous materials can be described as either rigid framed or elastic framed materials. Fiberglass and acoustical foams are considered elastically framed porous materials. All of these materials are heterogeneous in that they are comprised of a solid phase and a fluid phase as shown in Figure 2.2. The theory used here is similar to [3] as a macroscopic approach. The basic assumption is that the pore size (d) is much smaller than the macroscopic elementary volume of porous material (D1). Also, the wavelength (D2) of sound propagating within the porous medium is much larger than the pore space and the macroscopic elementary volume.

In the following, a Lagrangian approach together with finite element discretization is used to obtain the discretized equations of motion for a poroelastic medium. For a three-dimensional poroelastic element, six degrees of freedom per node are used. Three displacement components are for the solid phase and three others for the fluid phase.

2.2.1.a Poroelastic constitutive equations:

The constitutive equations of poroelastic material describe the stress-strain linear relation which is based on Biot-Allard model [4, 5], given as

$$\{\sigma_s\} = [D_s]\{\varepsilon_s\} + [D_{sf}]\{\varepsilon_f\} \tag{2.1}$$

and

$$\{\sigma_f\} = [D_f]\{\varepsilon_f\} + [D_{sf}]\{\varepsilon_s\} \tag{2.2}$$

where $\{\varepsilon_s\} = (\varepsilon^s_{xx}\ \varepsilon^s_{yy}\ \varepsilon^s_{zz}\ 2\varepsilon^s_{xy}\ 2\varepsilon^s_{yz}\ 2\varepsilon^s_{xz}\ )^T$ and $\{\varepsilon_f\} = (\varepsilon^f_{xx}\ \varepsilon^f_{yy}\ \varepsilon^f_{zz}\ 2\varepsilon^f_{xy}\ 2\varepsilon^f_{yz}\ 2\varepsilon^f_{xz}\ )^T$ are the strain vectors for the solid and fluid phase, respectively, and $[D_s]$, $[D_f]$, and $[D_{sf}]$ are the matrices of the

elastic coefficients related to the solid phase, the fluid phase, and their coupling strain, respectively. These matrices are written as

$$[D_s] = \begin{bmatrix} A+2N & A & A & & & \\ A & A+2N & A & & 0 & \\ A & A & A+2N & & & \\ & & & N & & \\ & 0 & & & N & \\ & & & & & N \end{bmatrix} \tag{2.3}$$

$$[D_{sf}] = Q\{m\}\{m\}^T \tag{2.4}$$

$$[D_f] = R\{m\}\{m\}^T \tag{2.5}$$

where A and N are Biot's coefficients corresponding to the Lame's coefficients in the theory of elasticity, and A is expressed as

$$A \cong 2N\frac{\nu}{1-2\nu} \tag{2.6}$$

Q is the Biot's coefficient for the elastic coupling between the solid and fluid phases. R is the Biot's coefficient for the bulk modulus of the fluid phase. The strain-displacement relations for the solid phase and the fluid phase are, respectively,

$$\{\varepsilon_s\} = [L]\{u\} \tag{2.7}$$

$$\{\varepsilon_f\} = [L]\{U\} \tag{2.8}$$

where [L] is the spatial derivative operator as

$$[L]^T = \begin{bmatrix} \frac{\partial}{\partial x} & 0 & 0 & \frac{\partial}{\partial y} & 0 & \frac{\partial}{\partial z} \\ 0 & \frac{\partial}{\partial y} & 0 & \frac{\partial}{\partial x} & \frac{\partial}{\partial z} & 0 \\ 0 & 0 & \frac{\partial}{\partial z} & 0 & \frac{\partial}{\partial y} & \frac{\partial}{\partial x} \end{bmatrix} \tag{2.9}$$

where {u} is the solid phase displacement and {U} the fluid phase displacement.

2.2.1.b Energy density functions

The equation of motion of a poroelastic system can be obtained from the energy functions of the system. These energy functions consist of the strain, kinetic, dissipation and work energy done by the applied loads. These energy function are described as follows:

1. Strain energy

The strain energy density for a poroelastic medium is given as

$$dU = \frac{1}{2}\left(\{\sigma_s\}^T\{\varepsilon_s\} + \{\sigma_f\}^T\{\varepsilon_f\}\right), \tag{2.10}$$

From the previous material constitutive equations and strain-displacement relations, the strain energy density term can be expanded into more meaningful expression as,

$$dU = \frac{1}{2}\left(([L]\{u\})^T[D_s][L]\{u\} + 2([L]\{u\})^T[D_{sf}][L]\times\{U\} + ([L]\{u\})^T[D_s][L]\{u\}\right) \tag{2.11}$$

The coupling between the strains of the frame and the fluid is represented by the middle term in Eq. (2.11).

2. Kinetic energy

The kinetic energy for a poroelastic medium is given by [5]

$$dT = \frac{1}{2}\left(\rho_{11}\{\dot{u}\}^T\{\dot{u}\} + 2\rho_{11}\{\dot{u}\}^T\{\dot{U}\} + \rho_{22}\{\dot{U}\}^T\{\dot{U}\}\right), \tag{2.12}$$

where u and U are solid and fluid phase displacements, respectively; ρ_{11} and ρ_{22} are the effective Biot's densities depending on the geometry of the poroelastic frame; ρ_{12} is related to the tortuosity of the frame.

3. Dissipation energy

The dissipation energy is introduced through the dissipation function [3],

$$dD = \frac{1}{2} b(\omega) (\{\dot{u}\} - \{\dot{U}\})^T (\{\dot{u}\} - \{\dot{U}\}), \tag{2.13}$$

where $b(\omega)$ is a complex and frequency-dependent viscous damping coefficient, and is related to the flow resistivity and tortuosity of the porous material. Also, the dissipation is proportional to the relative motion between the solid phase and the fluid phase.

4. External work energy

The external work done by the surface force is given as

$$dW = \{u\}^T (\{f\} - h\{f_n\}) + h\{U\}^T \{f_n\}, \tag{2.14}$$

where $\{f_n\}$ is the normal force vector. In Eq. (2.14) the first two terms and the last term are related to the solid and fluid phase, respectively.

2.2.1.c Finite element discretization

The continuous poroelastic system can be mathematically discretized into algebraic form for numerical computations. In order to do that, the interpolation functions are used to approximate the macroscopic displacement fields {u} and {U} in terms of their nodal displacements, for example, the *e-th* element mesh has the following form

$$\{u\}^e = [N_u]^e \{\bar{u}\}^e \text{ and } \{U\}^e = [N_U]^e \{\bar{U}\}^e \tag{2.15}$$

where $[N_u]^e$ and $[N_U]^e$ are the corresponding shape functions. The three-dimensional hexahedral shape function is illustrated in Figure 2.3. For an eight-node hexahedral or brick element, the Lagrange shape functions can be written as

$$N_i = \frac{1}{8}(1+\xi_i\xi)(1+\eta_i\eta)(1+\zeta_i\zeta) \tag{2.16}$$

where (ξ_i, η_i, ζ_i) represent the coordinates of node i (from 1 to 8) of the element in the (ξ, η, ζ) system. The generalized nodal displacements for the element are represented by the vector

$$q = [q_1, q_2, \cdots, q_{48}]^T \tag{2.17}$$

where each node has six degrees-of-freedom, three for solid phase and three others for fluid phase displacements.

Substituting Eq. (2.15) into all energy terms in Eqs. (2.11)-(2.14), summing those energy terms and integrating over the element, the discretized equations of motion for the poroelastic medium are in the matrix form as,

$$\left(-\omega^2\begin{bmatrix}[M_{ss}] & [M_{sf}]\\ [M_{sf}] & [M_{ff}]\end{bmatrix} + j\omega\begin{bmatrix}[C_{ss}(\omega)] & [C_{sf}(\omega)]\\ [C_{sf}(\omega)] & [C_{ff}(\omega)]\end{bmatrix} + \begin{bmatrix}[K_{ss}(\omega)] & [K_{sf}(\omega)]\\ [K_{sf}(\omega)] & [K_{ff}(\omega)]\end{bmatrix}\right)\begin{Bmatrix}u\\ U\end{Bmatrix} = \begin{Bmatrix}\{F_s\}\\ \{F_f\}\end{Bmatrix} \tag{2.18}$$

where [M], [C] and [K] are the equivalent stiffness, damping, and mass matrices, and the subscripts "*ss*", "*ff*" and "*sf*" denote solid phase, fluid phase and solid-fluid coupled phases inside the foam, respectively. The detailed expression of each sub-matrix is given in Appendix 1. In Eq. (2.18) the damping and stiffness matrices of the poroelastic medium are complex valued and frequency-dependent. Therefore, the final finite element system matrix is big and its frequency-dependent sub-matrices need to be calculated at each frequency. In general, the poroelastic elements occupy a significant portion of the system's degrees-of-freedom, and they require more lengthy computations when compared to other medium matrices.

2.2.2 Finite Element Formulation for Acoustical Medium

Consider a volume *V* enclosed by a surface *S*. Within the volume the pressure, p, must satisfy the wave equation

$$\nabla^2 p + \left(\frac{\omega^2}{c^2}\right) p = 0, \tag{2.19}$$

where ω is the angular frequency of vibration and *c* the speed of sound. On the acoustically hard surface the normal velocity is zero, giving

$$\partial p / \partial n = 0 , \tag{2.20}$$

The solution of the governing equation (2.19) subject to the boundary condition (2.20) can be written as an equivalent variational principle,

$$\delta \int_v \frac{1}{2} \left[(\nabla p)^2 - (\frac{\omega^2}{c^2})\, p^2 \right] dV = 0 , \tag{2.21}$$

In order to discretize the acoustic domain into classical finite element matrices, a three dimensional hexahedral shape function similar to poroelastic element (Figure 2.3) is used, which has only the pressure DOF per node. The pressure distribution is represented by a shape function as

$$p = \lfloor N \rfloor_i \{p\}_i \tag{2.22}$$

where

$$\{p\}_i = [p_1,\ p_2, \cdots,\ p_8]^T \tag{2.23}$$

is a column matrix of nodal pressure values for the *i-th* element.

The acoustical finite element formulation for the air cavity is based on Petyt's model [6]. The matrix equation for the acoustic enclosure is given as

$$\left(\frac{[K_a]}{\rho_a \omega^2} - \frac{[M_a]}{\rho_a c^2} \right) \{P\} = j \left\{ \frac{R}{\omega} \right\} \tag{2.24}$$

where $[K_a]$ is the stiffness matrix of the acoustic medium, $[M_a]$ the acoustic mass matrix (those are detailed in Appendix 2), *P* is the acoustic pressure, ρ_0 the air density, c the sound speed in air and the {R} the volume displacement of the air.

2.2.3 Finite Element Formulation of Elastic Plate

In deriving the energy functions for a thin plate, it is assumed that the direct stress in the transverse direction is zero. Also, normals to the middle surface of the undeformed plate remain straight and normal to the middle surface during deformation.

The kinetic and strain energy of the thin plate are given as [7],

$$T_e = \frac{1}{2}\int_A \rho h \dot{w}^2 dA \tag{2.25}$$

$$U_e = \frac{1}{2}\int_A \frac{h^3}{12}\{\chi\}^T [D]\{\chi\} dA \tag{2.26}$$

where

$$\{\chi\} = \begin{bmatrix} \partial^2 w / \partial x^2 \\ \partial^2 w / \partial y^2 \\ 2\partial^2 w / \partial x \partial x \end{bmatrix} \tag{2.27}$$

$$[D] = \begin{bmatrix} \frac{E}{1-\upsilon^2} & \frac{E\upsilon}{1-\upsilon^2} & 0 \\ \frac{E\upsilon}{1-\upsilon^2} & \frac{E}{1-\upsilon^2} & 0 \\ 0 & 0 & G \end{bmatrix} \tag{2.28}$$

The work done by external forces is

$$W = \int_s \left(p_x \delta u + p_y \delta v\right) ds \tag{2.29}$$

where s denotes the boundary of the element.

2.2.4 Finite Element Formulation of Piezoelectric Actuator

The active component of the smart foam system is the PVDF film that is embedded in the acoustic foam, and the PVDF film is driven by an electrical voltage that causes the film to strain.

The in-plane strain of the film is considered aligned with the electrical field and its strain energy density is expressed [3] as,

$$dV = \frac{1}{2} Y \left(\frac{du}{dx} \right)^2 + \frac{1}{2} \left(Y \frac{du}{dx} \right) \left(d_{31} E \right) \tag{2.30}$$

where Y is the Young's modulus of the PVDF film, d_{31} the piezoelectric strain constant, E the applied electrical field—voltage/thickness of PVDF.

The kinetic energy density of the in-plane motion of the PVDF film is described by

$$dT = \frac{1}{2} m_L \dot{u}^2 \tag{2.31}$$

where m_L is the mass per unit length of the PVDF film and $\dot{u}$ the axial velocity.

For numerical computation, the piezoelectric energy equation is discretized into matrix form via shape functions, $[N]^e$. The displacement field of the PVDF film, *{u}*, is in terms of the nodal displacement $\{\bar{u}\}^e$ for the e^{th} element,

$$\{u\}^e = [N_u]^e \{\bar{u}\}^e \tag{2.32}$$

For a two-dimensional piezoelectric film element the shape function is written as,

$$[N_u]^e = \left\lfloor \frac{1-\xi}{2}, \frac{1+\xi}{2} \right\rfloor, \tag{2.33}$$

and the three-dimensional shape function is

$$[N_u]^e = \frac{1}{4} \lfloor (1-\xi)(1-\eta), (1+\xi)(1-\eta), (1+\xi)(1+\eta), (1-\xi)(1+\eta) \rfloor \tag{2.34}$$

where ξ and η are finite element natural coordinates in x and y axes, respectively.

Substitutions of equations (2.33) and (2.34) into (2.30) and (2.31), the equation of motion for a piezoelectric actuator element is therefore, given by

$$\left([K] - \omega^2 [M] \right) \{u\} = \{F\} \tag{2.35}$$

where [K] and [M] are, respectively,

$$[K] = \int_e Y \frac{\partial}{\partial u}[N_u] \frac{\partial}{\partial u}[N_u]^T d\Gamma \tag{2.36}$$

$$[M] = \int_e \rho [N_u][N_u]^T d\Gamma . \tag{2.37}$$

The force vector is driven by a given voltage described as

$$\{F\} = Y d_{31} E \int_\Gamma \frac{\partial}{\partial x}[N] d\Gamma \tag{2.38}$$

Since the PVDF film is embedded in the acoustic foam, the mass and stiffness matrices and the forcing vector of the PVDF element will be added to the corresponding degrees of freedom of the foam.

2.3 FINITE ELEMENT COUPLING CONDITIONS

The coupling conditions involved in the smart foam system are of the following types: structural-acoustic, structural-poroelastic, poroelastic-acoustic, poroelastic-structural, and structural-acoustic-poroelastic.

2.3.1 Structural-Acoustic Coupling

The motion of the flexible wall is induced by the external pressure loads, and the motion of vibrating wall causes the acoustical medium inside the enclosed cavity to oscillate. This acoustic-structure interaction can be described by the following classical continuity equations [8],

$$\sigma_{ij} n_j = -P \delta_{ij} n_j \tag{2.39}$$

$$\frac{\partial P}{\partial n} = \omega^2 \rho_0 W_n \tag{2.40}$$

where *Wn* is the normal displacement of the vibrating structure. The compatibility of the normal force is ensured in (2.39) and the normal velocity ensured in (2.40) at nodal points at the interface joining the structural and acoustical system.

2.3.2 Structural-Poroelastic Coupling

When the poroelastic system is attached to a plate, there is continuity between the displacement field of the plate and that of the poroelastic material to be ensured at the nodal points at their interface. The interface conditions to be satisfied at the interface are [8]

$$u = W, \quad U_n = u_n \tag{2.41}$$

where u_n and U_n represent the normal displacement of the solid and fluid phases, respectively. The first equation ensures continuity of the solid displacements, while the second equation the continuity of the normal component of the acoustical flow. In the problems where rigid connections between the different media are required, we use the Lagrange multiplier method to treat constraints. The Lagrange multiplier adds constraint equation to the system but requires less matrix manipulations compared to the method of eliminating the dependent degrees of freedom.

2.3.3 Poroelastic-Acoustic Coupling

When the poroelastic material is coupled to a neighboring acoustic system, compatibility of the normal and shear forces and the continuity of the normal volume velocity should be ensured at the interface joints. Two types of interface conditions are considered here [8]. The first set of interface conditions model an open surface and the second set a sealed surface.

2.3.3.a Open surface interface conditions

At an open surface, there are four boundary conditions to be satisfied: two normal stress conditions, one shear stress condition, and a normal volume velocity condition. Those conditions are, respectively,

$$-hp = s \tag{2.42}$$

$$-(1-h)\,p = \sigma_x \tag{2.43}$$

$$\tau_{xy} = 0 \tag{2.44}$$

$$v_x = j\omega(1-h)u_x + j\omega h U_x \tag{2.45}$$

where h is the porosity of a foam.

2.3.3.b Sealed surface interface conditions

When the poroelastic material is bonded to a membrane, there are four boundary conditions that must be satisfied: one normal velocity condition, two displacement conditions, and a force condition. These conditions are

$$v_x = j\omega W \tag{2.46}$$

$$u_x = W \tag{2.47}$$

$$U_x = W \tag{2.48}$$

$$(\pm)\, p(\pm) q_p = -\omega^2 m_s W \tag{2.49}$$

where W is the membrane transverse displacement, m_s is the membrane mass per unit area and q_p is the normal force per unit area exerted on the membrane by the foam.

2.3.4 Actuator -Foam Coupling

In the case where the PVDF film is perfectly bonded to the structure, there are continuity of displacements between the PVDF film and the foam.

$$u_a = u_f \ , \quad v_a = v_f \tag{2.50}$$

where subscripts "*a*" and "*f*" denote the actuator and foam, respectively.

2.4 IMPLEMENTATION OF ACTIVE CONTROL IN SMART FOAM SYSTEMS

In order to devise an active noise control strategy using smart foam elements, the method of complex least squares is applied. The acoustic pressure is induced by two factors: external excitations and control excitations. In a mathematical expression,

$$\{P\} = \{P_e\} + [P_v]\{V\} \tag{2.51}$$

where,

$\{P\}$ = The total acoustic pressure state vector resulting from external excitations and control inputs.

$\{P_e\}$ = The acoustic pressure state vector due to external excitations.

$[P_v]$ = The acoustic pressure state matrix resulting from unit voltage input to the smart foams

$\{V\}$ = The unknown voltage input to the smart foams.

In order to compute the unknown voltage input that would minimize the total acoustic pressure, the following steps are taken. First, the total acoustic pressure vector is set to zero. Because the total pressure state vector is set to zero, the overall acoustic effect is global.

$$\{P_e\}+[P_v]\{V\}=\{0\} \tag{2.52}$$

Second, $[P_v]^H$, the hermitian of $[P_v]$, is multiplied to both the $\{P_e\}$ and $[P_v]$. This makes the resulting control-induced acoustic pressure matrix invertible. Finally, the unknown voltage is solved. The final expression of the unknown voltage for the global acoustic control is

$$\{V_G\}=-\left([P_v]^H[P_v]\right)^{-1}[P_v]^H\{P_e\} \tag{2.53}$$

This is an approximate minimization approach because the resulting $\{P\}$ due to $\{V_G\}$ is not null. When a set of multiple smart foams is used, $\{V_G\}$ can be used as a tool to identify the ones that are more effective than the others.

The next step taken is a development of a local control strategy. Mathematically, a pressure output vector is generated by multiplying Equation (2.51) with an output matrix $[C]$.

$$\{P_{output}\}=[C]\{P\} \tag{2.54}$$

where $\{P_{output}\}$ is an output acoustic pressure vector composed of pressures at pre-selected locations of sensors. It is a subset of the acoustic pressure state vector, $\{P\}$. Therefore, the output matrix $[C]$ extracts the information at the sensor locations from $\{P\}$. By substituting Equation (2.52) into Equation (2.54), the following expression of local minimization voltage is derived.

$$\{V_L\}=-\left([P_v]^H[C]^T[C][P_v]\right)^{-1}[P_v]^H[C]^T[C]\{P_e\} \tag{2.55}$$

2.5 THE COMPLETE COUPLED FINITE ELEMENT SYSTEM

The completely coupled system consists of structural, acoustic, and poroelastic elements and their related coupling matrices where interface conditions are established. In this present study, the 4-noded rectangular element is used for the plate element. This plate element has three degrees of freedom at each node, namely, the normal displacement and two rotations. As for the acoustic cavity, the 8-noded isoparametric hexahedron element with one pressure degree of freedom is used. A similar hexahedron element for the poroelastic medium is used, but it has 6 degrees of freedom per node (three translations for the solid phase and three for the fluid phase). Combining each individual element and their corresponding coupling matrices, the coupled system is established. For example, in the case of a plate/air/porous/plate configuration, the coupled system is given as

$$\begin{bmatrix} [plate1] & [pl1/air1] & [0] & [0] & \lceil l \rceil \\ [pl1/air1]^T & [air1] & [fo1/air1]^T & [0] & \lfloor a \rfloor \\ [0] & [fo1/air1]^T & [foam] & [fo1/pl1]^T & \lfloor g \rfloor \\ [0] & [0] & [fo1/pl1] & [plate1] & \lfloor \vdots \rfloor \\ [lagrange & constra\,\text{int} & matrix & \cdots] & [0] \end{bmatrix} \begin{Bmatrix} D_{p1} \\ D_a \\ D_f \\ D_{p2} \\ D_l \end{Bmatrix} = \begin{Bmatrix} F_{p1} \\ F_a \\ F_f \\ F_{p2} \\ 0 \end{Bmatrix} \tag{2.56}$$

where [plate1] and [plate2] are plate system matrices, [foam] the poroelastic matrix, [pl1/air1] the coupling matrix for plate 1 and air cavity 1, same matrix notations applied to [fo1/air1] and [fo1/pl1]. The Lagrange constraint matrix is utilized for rigid connections between foam and plate. Due to the frequency-dependent nature of poroelastic material, the foam system matrix needs to be updated for each frequency, which is the most time consuming portion in the whole computation process and it happens only to the poroelastic element.

2.5.1 Sound Transmission Loss

The sound transmission loss is evaluated as

$$TL = 10\log\left(\frac{I_i}{I_t}\right) \tag{2.57}$$

where $I_i = p_{rms}^2 / (4\rho_a c)$ is the normal intensity incident on the panel, P_{rms}^2 is the space-average, mean square sound pressure in the reverberation room, and I_t is the transmitted normal intensity averaged over the surface of the test panel.

2.6 NUMERICAL VALIDATIONS AND DISCUSSIONS

The finite element model described in the previous sections was coded in Matlab script language and executed under the Matlab environment. The sound transmission loss program based on Rayleigh integral and mesh generator programs were written in C language. Matlab was chosen to develop the program because of its rich math library and pre-coded control algorithms. However, Matlab codes are written in script language which may not be executed as fast as compiled machine codes, such as programs writtrn in FORTRAN, C and C++.

In the following, the program is used to make predictions for foam medium, foam-air coupled system, and double-panel cases with bonded-bonded foam configurations. The results are compared with results in the existing literature as a means of validating the finite element model.

2.6.1 Surface Impedance of Poroelastic Material

The prediction of surface impedance of poroelastic material is used to validate the poroelastic finite element model. The prediction is compared with an exact analytical calculation in [10]. The configuration of poroelastic layer is depicted in Figure 2.4a, the material properties are described in Table 2.1. The glass wool layer is bonded to a rigid impervious wall, and a normal incidence plane wave of unit amplitude excites the absorbing material. Since the layer is assumed laterally infinite, only the axial displacement is considered and the lateral displacement is set to zero. The poroelastic layer is modeled with ten 8-noded hexahedral elements in Figure 2.4b. The finite element prediction provides excellent results when compared with the exact solution, shown in Figure 2.5, and proves the validity of the developed poroelastic element.

2.6.2 Absorption Coefficient of Poroelastic Material

In order to validate the accuracy of the coupled poroelastic/acoustic finite element model, a three-dimensional waveguide containing foam and air elements is used, shown in Figure 2.6a.

The material properties of the foam are listed in Table 2.2. The predicted absorption coefficient of the foam is compared with the result from [7]. In this case, a plane acoustic wave is traveling toward the foam, and the surface velocity on the foam surface can be calculated from the finite element model. Once the surface velocity of the foam is predicted, the same approach described earlier can be used to compute the surface impedance Z_n. The absorption coefficient is then obtained through the following equation

$$\alpha = 1 - \left| \frac{Z_n - \rho_a c}{Z_n + \rho_a c} \right|^2 \tag{2.58}$$

In this validation, the finite element prediction is compared with a previously validated 2-D model, as shown in Figure 2.6b. The previous 2-D finite element has been validated against the analytical solution in [8]. An excellent agreement between both is obtained, and it validates the developed coupling matrix between poroelastic and acoustic media.

2.6.3 Sound Transmission through a Double-Panel System

In this section, the validation of the panel vibration and sound radiation is presented. Air is the only medium inside the double-panel cavity. The finite element model for this air-filled double-panel is depicted in Figure 2.7a. The normal incidence transmission loss through a double-panel is used to validate the plate, acoustic elements and their structure-acoustic coupling matrix all together. The sound transmission loss is based on the Rayleigh's integral method which needs the finite element solution of surface velocities of plate 2. Comparison between the finite element prediction and the published data from [9] is shown in Figure 2.7b, and the good agreement validates the structure-acoustic finite element model.

2.6.4 Double-Wall Panel with Bonded-bonded Foam

A double-panel system with bonded-bonded foam configuration is presented to study the coupling between panels and the foam. The foam is assumed perfectly attached to the flexible panels. Material properties and dimensions are listed in Table 2.3. The finite element model for this design configuration is shown in Figure 2.8a. A uniform acoustic pressure is applied to plate 1 as the only external force to the system. Plate 2 vibrates and radiates sound caused by the coupling of foam and plate 1. The finite element prediction is close to the published data [9],

and differences are less than 5 dB, see Figure 2.8b. This agreement would likely be improved with a higher mesh density model. When this finite element model is compared with the previous air filled model the previous one has much higher mesh density than the current model. Obviously, the foam model needs a higher density than the acoustic system because of its complex physical mechanism and its 6-DOF node containing both solid and fluid phases. However, a higher mesh density for this foam model results in a substantial increase in computation time, so there is a trade between accuracy and speed which must be taken into account when one makes predictions for FE models with foam elements.

This example can be extended to model a Distributed Vibration Absorber (DAV) system, if one of the plates bonded to the foam does not have any constraints. A DVA system can be tuned by varying the mass distribution or stiffness distribution of this plate in order to minimize the vibration of the structure and therefore reduce the noise. Moreover, if an active PVDF film is embedded in the foam, a Distributed Active Vibration Absorber (DAVA) is created.

2.6.5 Active Control in a 2-D Smart Foam System

A subsection in the main MATLAB file is created to implement the active control strategies and a simple case is tested to determine their effectiveness. The tested finite element model is shown in the Figure 2.9. It consists of 3 smart foam elements placed in the bottom of an air duct. The external excitation is a line volume velocity source of 0.002 m^3/s and this represents a noise source with 80dB SPL. Figure 2.10 shows the response of the duct without any control input at 80 Hz. Figure 2.11 shows the response of the duct after implementing the global control strategy at 80 Hz. As the two figures indicate, the overall reduction ranges from about 10 to 40 dB.

In order to study the effectiveness of the local minimization strategy, a strip between the smart foams and the noise source is chosen as a sensor location. Figure 2.12 shows the duct response after applying $\{V_L\}$. As the figure clearly indicates, the control strategy is highly effective in reducing the noise within the chosen zone. And, unlike the global reduction strategy, the local control effort is clearly more effective in terms of the level reduction within a selected zone because of the fewer number of the pressure variables to minimize.

To observe the performance of the smart foam elements, the computed applied voltages are plotted. Figure 2.13 shows the computed voltages for both the global and local control strategies

in the frequency range from 5Hz to 50 Hz. As expected, the control effort is significantly higher in the low frequency region for both the strategies. Generally, the local control takes more effort than global control throughout the frequency range. Also, Foams 1 and 3 show identical trends. This indicates that the computed voltages actuate the foams in spatially symmetric manners. In terms of magnitude, the voltage for the Smart Foam 2 shows higher levels for both the control strategies, thus playing a more critical role in reducing sound pressure than its neighbors. Consequently, a control strategy can be devised to take advantage of this factor, which would reduce the overall control level. Finally, the local control strategy shows a modal behavior around 280 Hz. The cause is still under investigation.

2.7 CONCLUSIONS

In this section, the development of a three-dimensional finite element model for a coupled PVDF-structure-acoustic-poroelastic smart foam system is described. Predictions can be made using this smart finite element model for a variety of configurations ranging from systems with single medium to systems made of elastic, acoustic, and poroelastic media. For a single medium system, the program predicts surface impedances of the foam, cavity pressures and structural responses, and for a multiple media coupled system the program can predict sound absorption coefficients and sound transmission loss for a simple double-panel or that with different foam lined configurations. A step-by-step approach was taken in building the smart foam finite element model from individual medium elements to multiple coupled interface matrices along with their corresponding validations.

Except for the foam lined case which may need refined meshes to improve accuracy, this finite element model predicts results which agree very well with published data. Those validations verify implementations of mathematical equations on which the finite element model is based. In the future, the capability of the smart foam finite element model will be improved to handle detailed models more efficiently without losing accuracy, by applying techniques such as DOF reduction of foam elements where lateral DOF's can be mathematically ignored under certain conditions.

The finite element model can be used for other complex boundary conditions, geometries, excitations, and different liner designs. The smart foam model development will be continued, and the three-dimensional PVDF element will be developed and integrated in the present foam system. Further, the design parameters of the smart foam element, including the dimensions, shapes and material properties of the foam and the PVDF actuator, can be determined by using this model to achieve the noise reduction in the frequency range of interest.

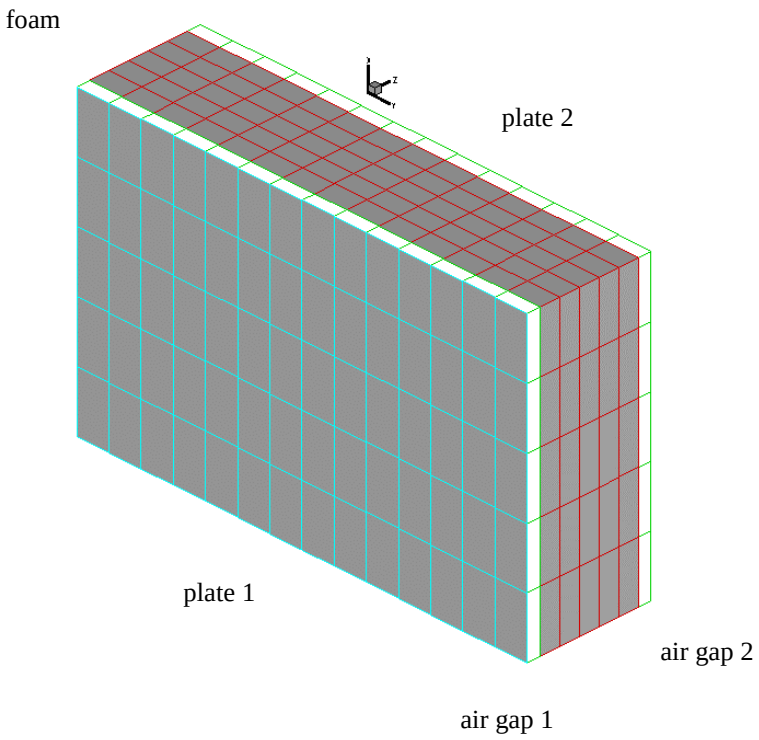

Figure 2.1 Geometry of the coupled plate/air/foam/air/plate problem

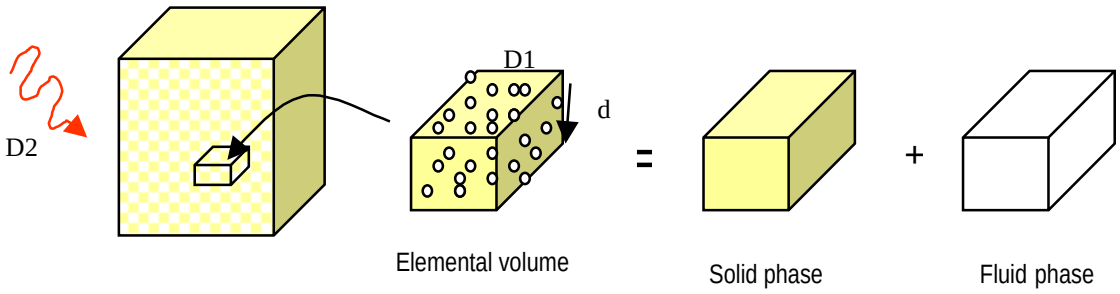

Figure 2.2 Macroscopic Modeling of Smart Foam

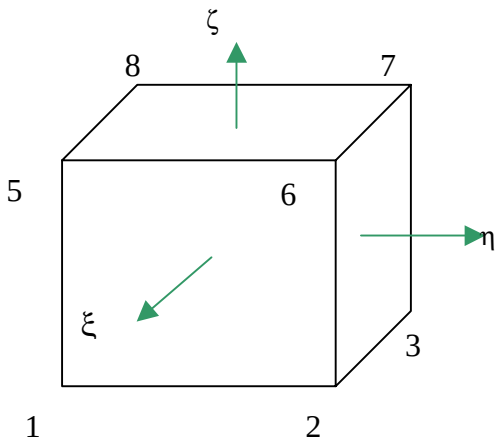

Figure 2.3 Geometry of 8-noded isoparametric hexahedra element

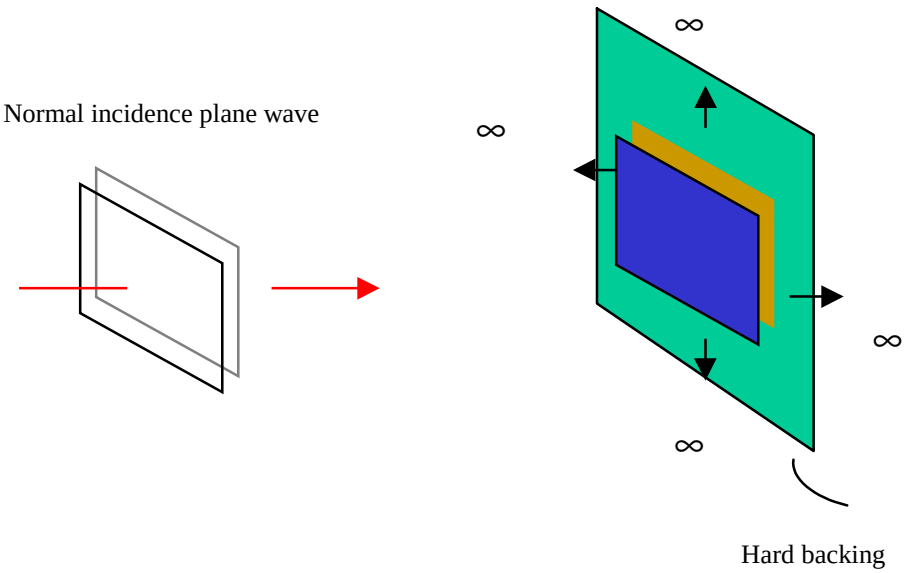

Figure 2.4a. Geometry of the surface impedance problem

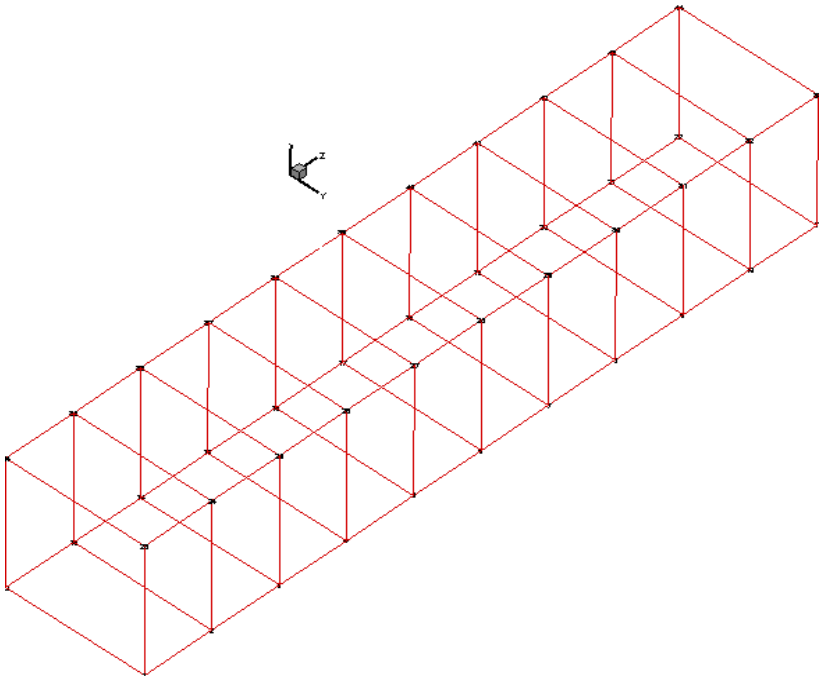

Figure 2.4b. Finite element model of the surface impedance problem

Table 2.1. Physical properties and dimensions of the glass wool material

Glass wool	
Tortuosity	1.06
Solid mass density	130 kg/m^3
Flow resitivity	40000 Nm^{-4}s
Porosity	0.94
Shear modulus	220(1+0.1j) N/cm^2
Viscous characteristic dimension	56 *u*m
Thermal characteristic dimension	110 *u*m
Thickness	10 cm

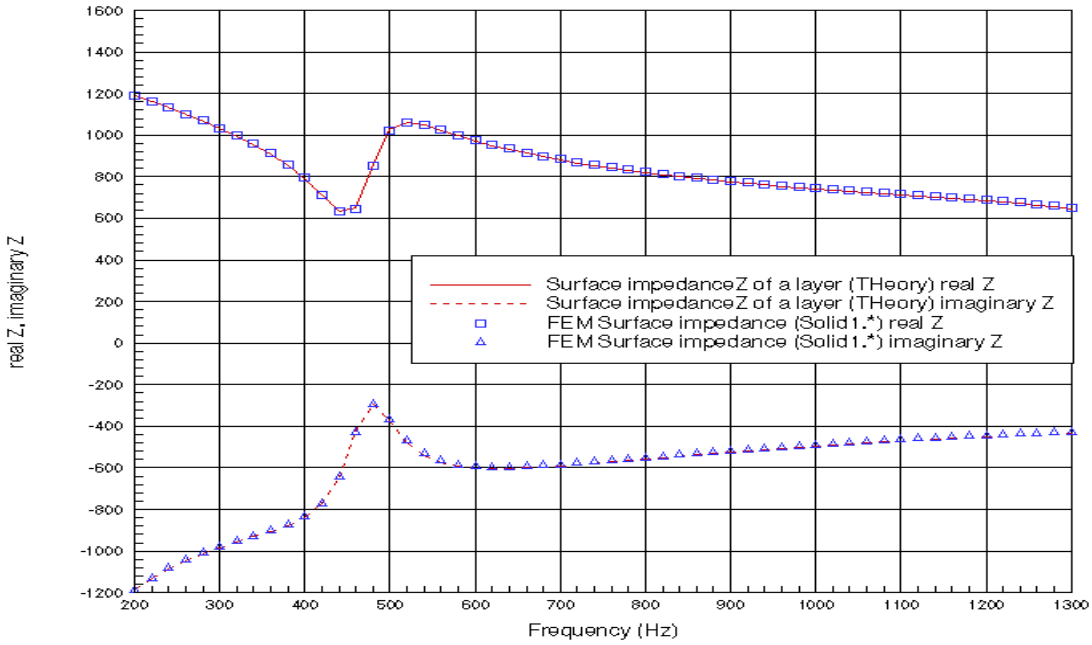

Figure 2.5 Comparison of the surface impedance between an analytical model and the finite element model for the glass wool layer

Table 2.2. Physical properties and dimensions of the Poroelastic foam material

Poroelastic foam	
Tortuosity	7.8
Solid mass density	30 kg/m^3
Flow resitivity	25000 Nm^{-4}s
Porosity	0.90
Young's modulus	8.0E5 N/cm^2
Poission's ratio	0.4
Loss factor	0.265
Thickness	40.5 cm

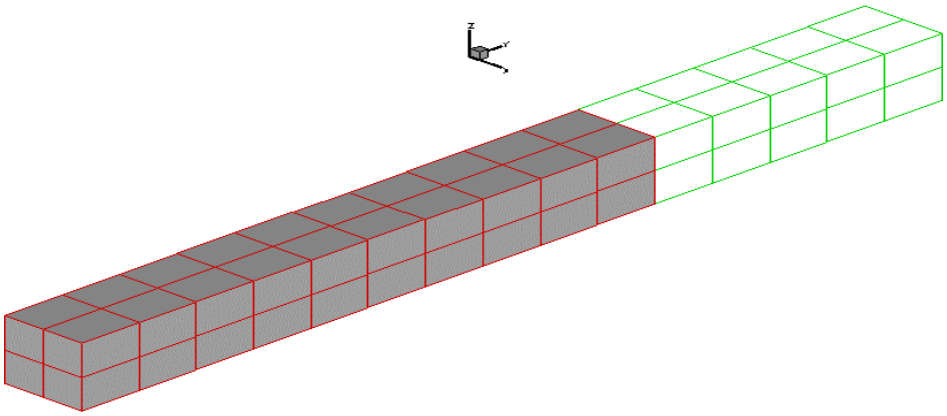

Figure 2.6a. Finite element model of the sound absorption coefficient problem, foam elements are in dark area, and others are air elements

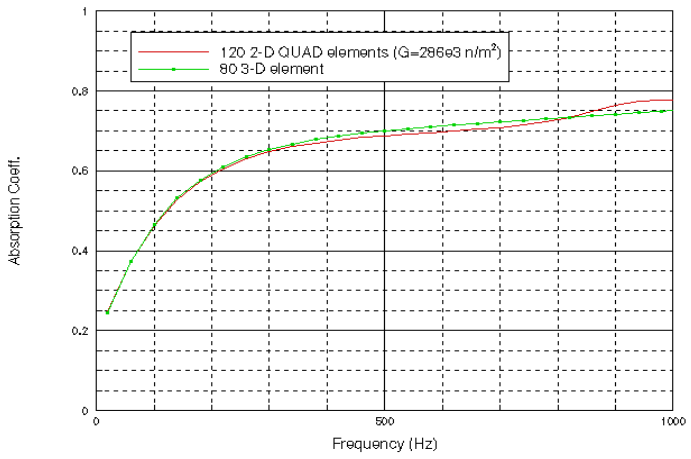

Figure 2.6b. Comparison of the absorption coefficient between a previously validated 2-D finite element model and the current 3-D model

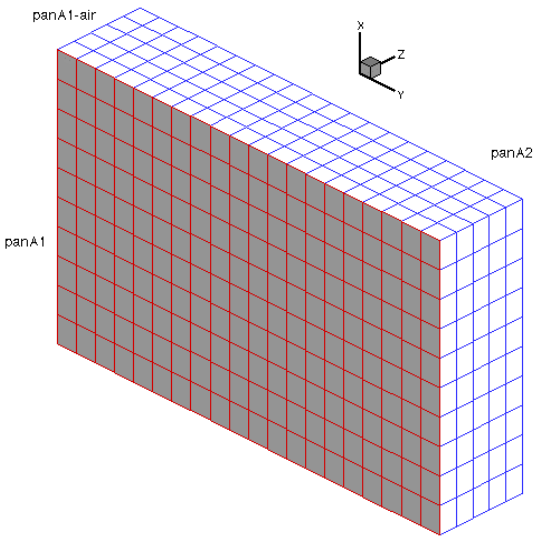

Figure 2.7a. Finite element model for the air-filled double wall system

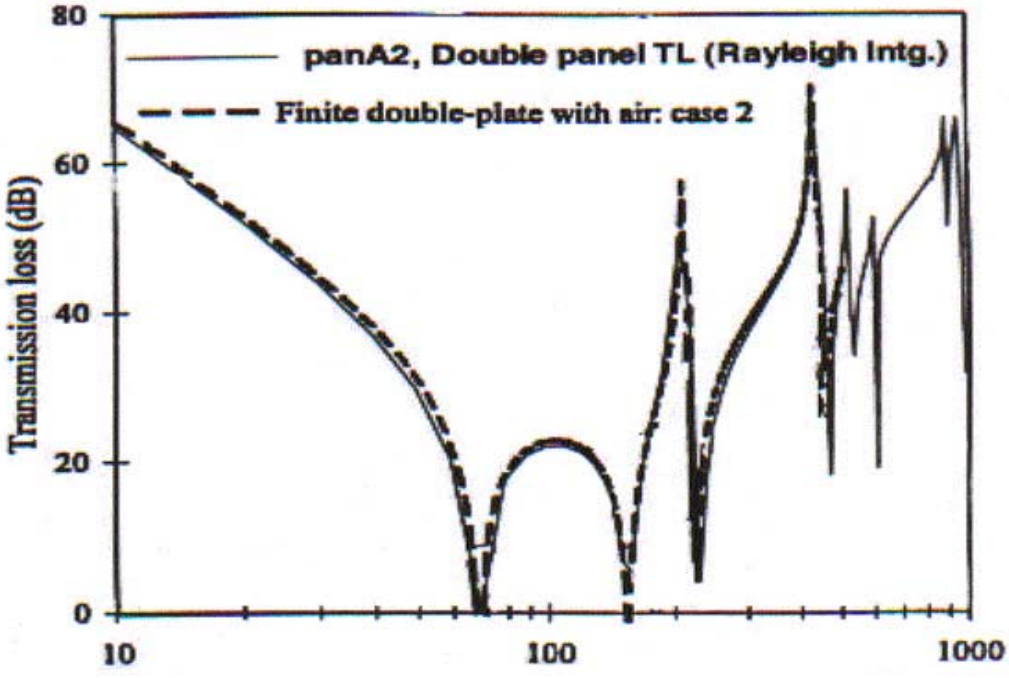

Figure 2.7b. Comparison of the normal incidence sound transmission loss through an air-filled double panel between the FE prediction,---, and results from [9], - - -

Table 2.3, Physical properties and dimensions for a double-panel system

Plates	
Width	0.35 m
Height	0.22 m
Thickness	0.001 m
Mass density	2814 kg/m^3
Young's modulus	71 Gpa
Acoustic pressure	1.0 N/m^{-2}
Poisson's ratio	0.33
Loss factor	0.01
Foam	
Depth	0.0762 m
Flow resistivity	25000 Nm^{-4}
Porosity	0.90
Tortuosity	7.8
Viscous characteristic dimension	93.2 *u*m
Thermal characteristic dimension	93.2 *u*m
Poisson's ratio	0.4
Bulk modulus	800 kPa
Loss factor	0.265
Solid mass density	30 Kg/m^3

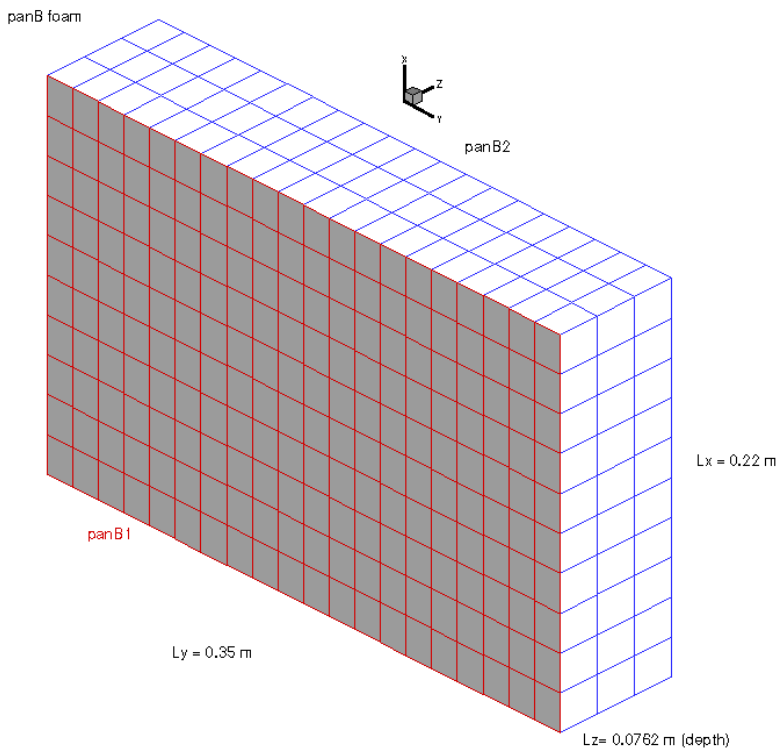

Figure 2.8a. Finite element model for the double wall system with bonded-bonded foam configuration

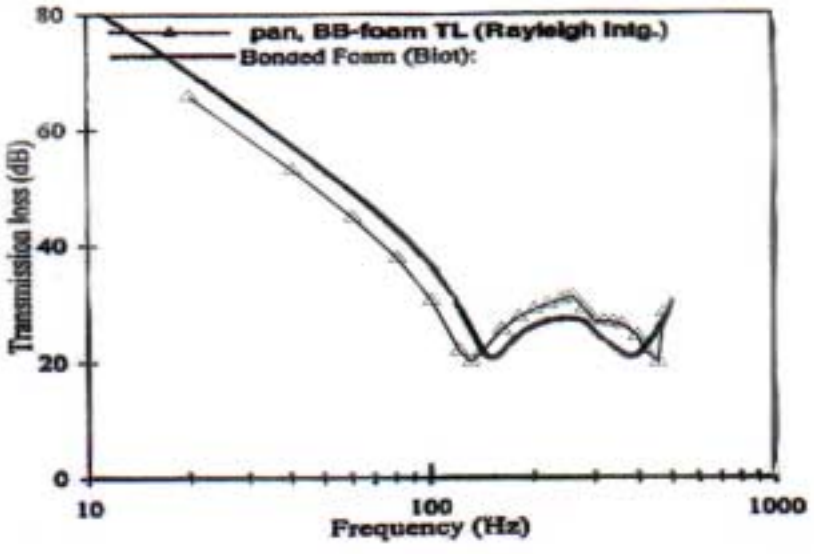

Figure 2.8b. Comparison of the normal incidence sound transmission loss through a double-panel with bonded-bonded foam: FE prediction,--ρ-, and result from [9], ---

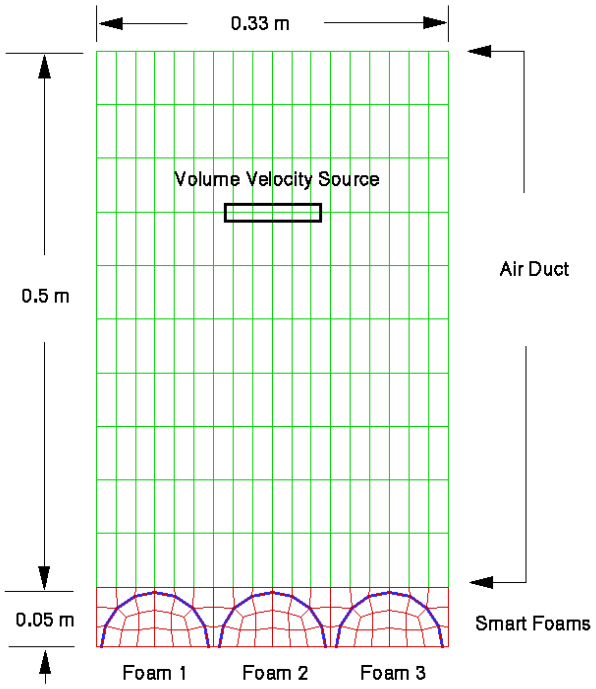

Figure 2.9 The finite element model for active control implementations

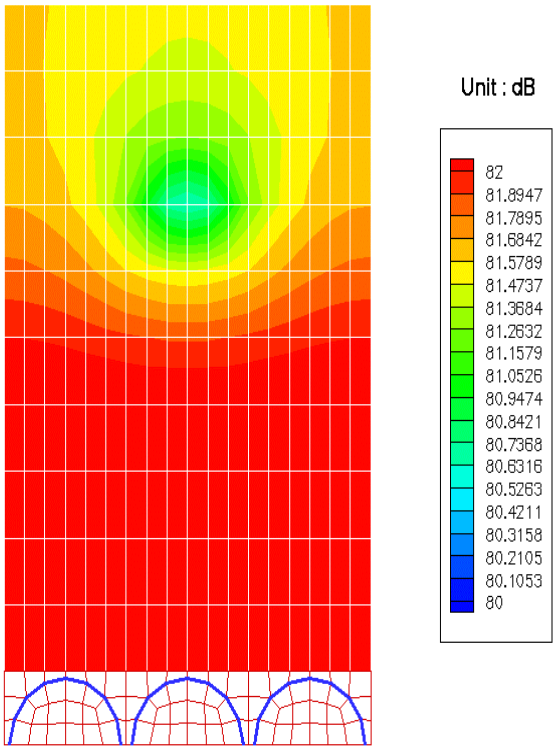

Figure 2.10 The response of the air duct without control

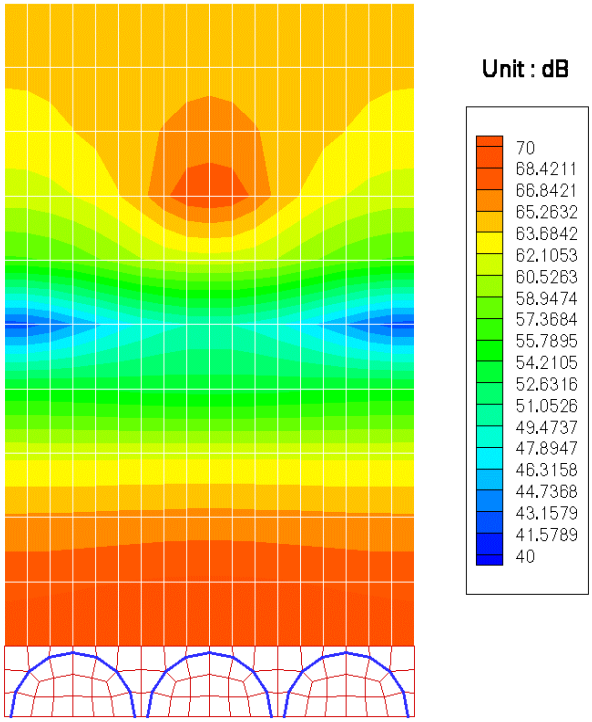

Figure 2.11 The response of the air duct with the global control at f=80 Hz

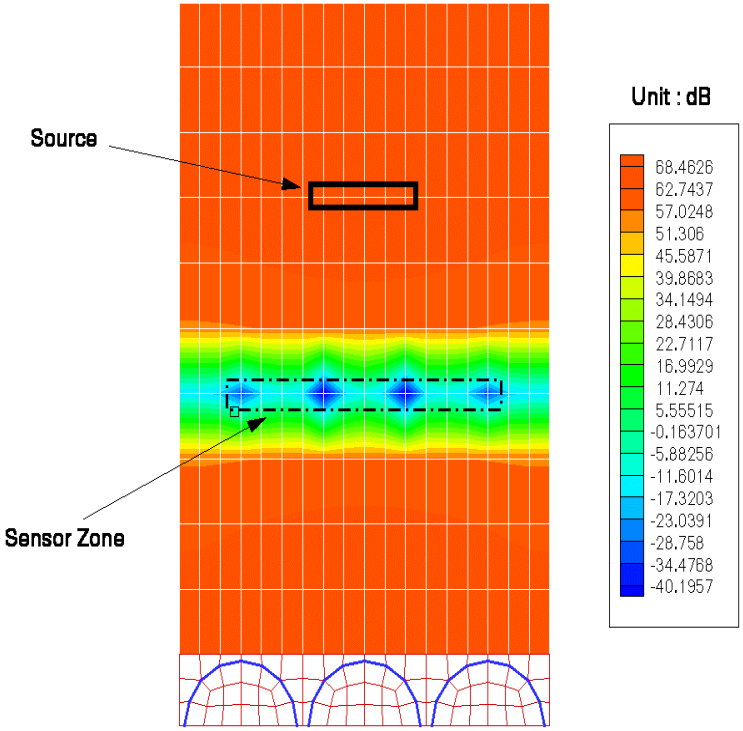

Figure 2.12 The response of the air duct with the local control at f=80 Hz

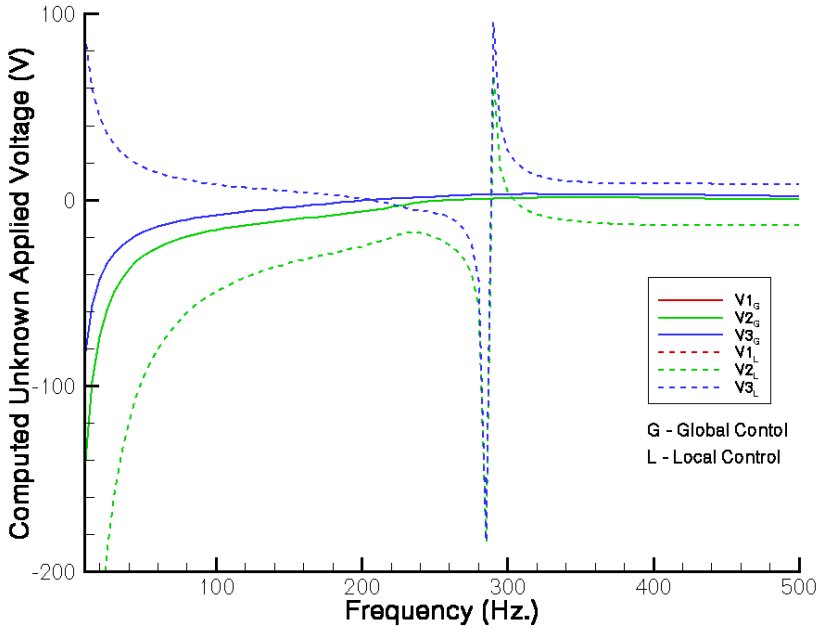

Figure 2.13 Computed applied voltages for the smart foam actuators due to the control strategies

3. SMART FOAM TESTS

The development and testing of an aircraft sidewall treatment using smart foam lining is discussed in this section. In the first phase, laboratory experiments were conducted on a double wall panel system to evaluate acoustic performance of several passive and active configurations of smart foam actuators attached to the base panel. In the second series of tests, active control using smart foam actuators was implemented on a 757-sidewall section configured with a trim panel. A multi-input, multi-output (MIMO), filtered-X, feed-forward controller with realistic reference sensors (e.g., accelerometers) was used to accomplish active control through the smart foam elements by minimizing the error signal provided by an array of error microphones. The active control through smart foam actuators significantly improved noise reduction of the sidewall in the low to mid frequency range (200 – 800 Hz).

3.1 INTRODUCTION

In recent years, there has been an increasing interest in the reduction of sound and/or vibration by use of hybrid active-passive control techniques. Smart foam is a composite noise control treatment that consists of a distributed piezoelectric actuator, known as polyvinylidene fluoride (PVDF), embedded within a layer of partially reticulated polyurethane acoustic foam. Passive acoustic foams offer a very reliable high frequency sound reduction method. Embedding piezoelectric actuators in the foam enhances the noise reduction characteristics of the foam through active control in the low frequency region. The resultant smart foam combines the inherent mid- to high-frequency passive noise control capability of an acoustical foam treatment with the low frequency noise control capabilities of an active control system. This active noise control approach utilizes and integrates the passive sound proofing subsystem as part of the active system to conserve weight and space.

Bolton et al [11], Fuller et al [1,12,13], have investigated the effectiveness of smart foam actuators for reducing sound radiation from vibrating panels. In these previous investigations, smart foam actuators were directly bonded to the vibrating structures and tested for different excitation fields, such as acoustic and boundary layer noise. Mathur et al [14] examined the

effectiveness of smart foam lined trim panels in improving transmission loss of a fuselage sidewall. In the present work, the emphasis is on the design and testing of a configuration of smart actuators which can be integrated into the noise reduction treatment package of a fuselage sidewall.

3.2 EXPERIMENTAL SETUP

These tests were divided into two groups: (i) active control of broadband sound radiation from a flat, stiffened panel and (ii) active control tests on the 757 fuselage sidewall. Both of these configurations incorporated a trim panel, thereby creating a double wall system. In the first tests, the main objectives were to: (1) investigate the effects of different reference sensors and select the most effective reference sensor strategy, and (2) optimize controller configuration. The main objective of the second tests was to incorporate the lessons learned from the first tests to demonstrate significant active control of broadband noise transmission through a full-scale fuselage.

In the first series of tests, a flat, stiffened panel was mounted in the test window of a transmission loss suite consisting of two reverberation chambers at VPI&SU (Virginia Polytechnic Institute & State University, Blacksburg VA). An illustration of the test setup is shown in Figure 3.1. Four smart foam actuators were bonded to four sub-panels of the stiffened panel, see Figure 3.2. A trim panel, attached to the frames of the stiffened panel, created the double wall system and covered the smart foam actuators. The sound field in the source room was monitored by 3 microphones placed at random locations. Four microphones were placed in the double wall cavity. Eight far-field and 4 near-field microphones were used for control and measurement in the receiving room. Twelve accelerometers, three on each of the four sub-panels with smart foam actuators, provided realistic reference signals.

In the active control tests, the performance of smart foam was compared with and without control. The effect of controller configuration on smart foam performance was also investigated. Several other parameters, such as number and placement of smart foam actuators, reference

signal and number of control channels, were studied during the tests. The instrumentation layout for active smart foam tests is shown in Figure 3.3.

In the second series of tests, a sidewall section of a 757 fuselage was mounted in the test window (see Figures 3.4a and 3.4b) of the Interior Noise Test Facility (INTF) located in the Boeing ANP (Aerodynamic, Noise and Propulsion) Engineering Laboratory complex in Seattle. This sidewall section includes the sidewall, floor and cargo compartment and extends over four frame bays. Within the INTF, a reverberation chamber, with a dimension of 35 x 29 x 23 feet, houses the source speaker system. An anechoic chamber, with a dimension of 58 x 41 x 31 feet, was used to measure the transmitted sound through the structure.

The receiving side of the fuselage panel with the trim removed is shown in Figure 3.5a. The smart foam tests reported here were limited to an area encompassing three frames and six longerons as shown. The other areas were treated with acoustic foam and lead vinyl blankets to reduce the flanking of acoustic energy via this path. The corresponding trim panels were located over these areas as well. For all the tests the overhead baggage containers were located in position as shown. The arrangement of smart foam elements and DVAs, used to control the sound transmission, is illustrated in Figure 3.5a. Four smart foam actuators numbered 1 through 4 were located above the window plane as shown. Four additional smart foam actuators numbered 5 through 8 were also located along the floor line. Twelve DVAs with tuned frequencies in the frequency range of 350 -450 Hz were located as shown in Figure 3.5a. A close up photo of the smart foam element (#2) and DVA combination located above the window line is shown in Figure 3.5b. Note that the smart foam elements do not completely cover the panel as desired. This is due to limitations in the number of usable control channels for a fully coupled controller. It is observed that the lack of continuous smart foam coverage is likely to reduce the obtained performance.

A random, diffuse sound field of approximately 100 dB over a frequency range of 100 – 1000 Hz, with a peak at 450 Hz, was set up in the reverberation chamber. A shaker was attached to the fuselage section (on the source side) in the window belt area for the case of structural excitation. A microphone array containing 10 microphones was installed in the anechoic chamber. Four additional monitoring microphones were placed in the anechoic chamber at

different heights and distances from the test panel. Several configurations of smart foam actuators on the sidewall were tested.

An acoustical grade, partially reticulated polyurethane open cell foam, designed to give maximum sound absorption per given thickness, provided the passive element of the smart foam. Since passive noise reduction is only significant at high frequencies, a PVDF film was embedded in the foam to implement the active control, which is most effective at low frequencies. The active PVDF film forces both the fluid and solid phases of the acoustic foam. The PVDF film is intentionally curved to couple the predominantly in-plane strain associated with the piezoelectric effect and the out-of-plane motion, which is the dominant mechanism of radiating sound away from the surface of the foam. Much work has been done to investigate the optimal configuration of a smart foam actuator [3]. In this investigation, smart foam actuators were constructed with the PVDF film curved into a half cylinder form along the length of the actuator and is embedded in two foam halves with a spray adhesive.

3.3 DISCUSSION OF RESULTS

3.3.1 Flat, Stiffened Panel Tests

A 4x4x4 controller configuration with four input channels (e.g., error sensors), four output channels to drive four actuators and four reference sensors (except for the ideal reference) was used for active control tests. The bandwidth of active control was kept in the frequency range of 200 – 630 Hz. The ideal reference, taken from the wide-band noise generator, was initially used in the active control experiments. Figure 3.6a shows a comparison of the sound field measured at 4 error microphones for control on and off conditions. With the ideal reference, significant reduction in the noise radiated by the double panel was achieved at the 4 error sensor locations. The noise reduction, mostly between 200 – 500 Hz, achieved at eight far field monitoring microphones is shown in Figure 3.6b.

A practical reference sensor scheme, which involved four accelerometers mounted on the stiffened panel, was used with the 4 x 4 x 4 controller configuration. In this setup, significant noise reduction in the frequency range of 200 – 700 Hz was achieved at 4 far-field control

microphone locations, see Figure 3.7a. The noise reduction at all eight monitoring microphones, however, was confined to some of the peak pressures (Figure 3.7b).

In the next setup, four near-field microphones were used in place of far-field sensors. The noise reduction achieved at four near-field error sensors is shown in Figure 3.8a, whereas the noise reduction at eight far field monitoring microphone locations is illustrated in Figure 3.8b.

In the next configuration, four cavity microphones were used as reference sensors with the same 4 x 4 x 4 controller configuration. Although significant noise reduction was achieved at four cavity error microphones, as shown in Figure 3.9a, it did not result in any noise reduction at eight far-field monitoring microphones (see Figure 3.9b).

In an effort to improve controller effectiveness, the control bandwidth was set in the frequency range of 315 – 630 Hz. The noise reduction achieved at four far-field error microphones for the case of four accelerometer reference sensors is shown in Figure 3.10. When compared with Figure 3.7a, the noise reduction achieved at four error sensors improved considerably due to a reduction in the control bandwidth.

These laboratory tests conducted on a double-panel system demonstrated that: (1) smart foam actuators can provide global sound reductions of transmitted broadband noise, (2) feed-forward control approach using realistic sensors (i.e., accelerometers) located on the base panel can be used for broadband noise control for such systems, and (3) control voltages for smart foam actuators were typically in the range of 30 – 50 V rms.

3.3.2 Fuselage Sidwall Tests

The flat, stiffened panel tests showed that the most effective strategy for broadband noise reduction through double wall systems is to use a 4 x 4 x 4 controller configuration with accelerometers mounted on the stiffened panel as error sensors. This approach was used in the fuselage sidewall tests. The middle two frame bays of the757 sidewall section, shown in Figure 3.3, were used as the test area for active noise control. The outer two frames bays of the sidewall section were treated with insulation, trim panel and two layers of mass fabric to reduce flanking sound transmission through these sections.

Eight smart foam cells were placed on four sub-panels. The actuators were wired in pairs, effectively making 4 control channels out of 8 smart foam actuators. The smart foam tests were

conducted in several steps. First, the effectiveness of controller configuration and reference sensors on noise reduction was investigated on the fuselage sidewall without the trim panel. The controller performance improved by increasing the number of system ID coefficients, number of controller coefficients and sampling frequency.

In the first case, active control tests were conducted on the fuselage sidewall with the smart foam actuators but without the trim panel. Three accelerometers on each of the sub-panels provided the reference signals for the controller. A marked improvement in the noise reduction or attenuation in the control bandwidth of 200 – 800 Hz was achieved with active control over the error sensors (see Figure 3.11). Peak attenuations of greater than 10 dB and a total of 5 dB over the bare panel were achieved.

The trim panel was then added to the sidewall. The noise reduction achieved with 4 x 4 x 4 controller is shown in Figure 3.12. The use of four accelerometers as reference sensors with four coupled smart foam actuators resulted in about 7 – 10 dB noise reduction over the control bandwidth of 200 –700 Hz (see Figure 3.11). Control voltages were typically 50 – 90 V rms for the source levels described previously.

The results for structural excitation (e.g., shaker excitation) are summarized for comparison purposes in Figure 3.13. Significant reductions in the averaged sound pressure levels were achieved at control microphones, with a total reduction across the 200 to 800 Hz bandwidth of 6dbB. It is again evident that the smart foam/DVA treatment leads to significant active/passive reduction in broadband radiated sound from the 757-fuselage panel.

3.4 CONCLUSIONS

Extensive laboratory tests were conducted on several configurations of active smart foam actuators attached to a flat stiffened panel and a stiffened fuselage sidewall. The following conclusions may be drawn based on these tests: (i) significant improvement in noise reduction of the test panel and the 757 fuselage section were observed for both acoustic and structural excitations due to active control with smart foam actuators, (ii) accelerometers on source plate provide very good references for the controller, (iii) the 4 x 4 x 4 controller configuration was effective for achieving significant reductions at error sensors, (iv) control strategies using far-

field microphones as error sensors lead to very good broadband attenuation, but more error sensors/actuators would be needed to control the sound pressure over the entire receiving room at high frequencies, (v) good attenuation at near-field microphones allows some attenuation at far-field microphones, (vi) strategies using error microphones in cavities and accelerometers as volume velocity sensors are not working well on the far-field attenuation at the present time; further investigation are needed for those cases.

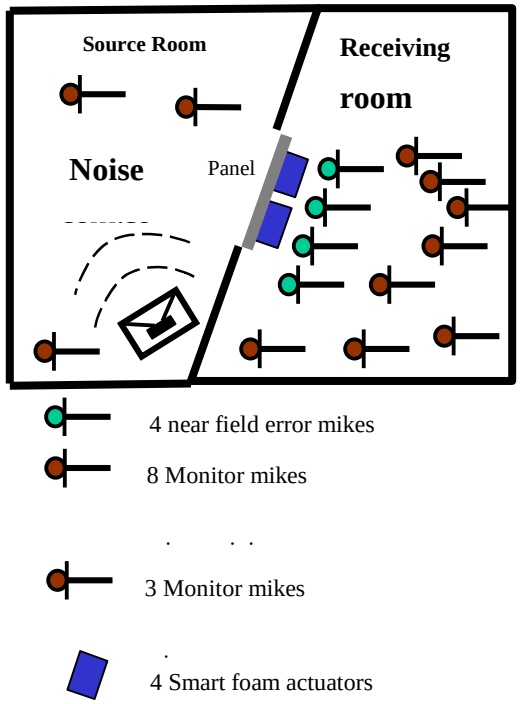

Figure 3.1. Laboratory setup showing smart foam actuators, error sensors and monitoring microphones.

Figure 3.2 Stiffened panel with four smart foam actuators.

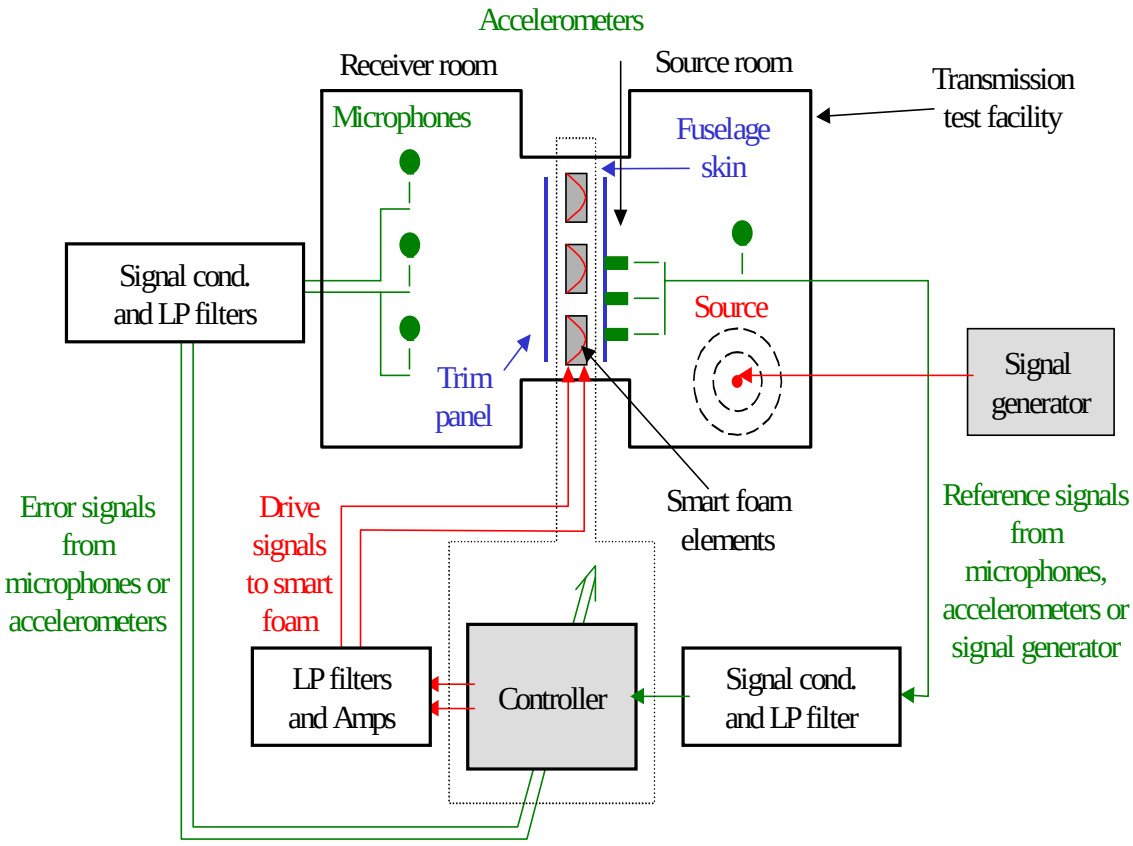

Figure 3.3 Instrumentation layout.

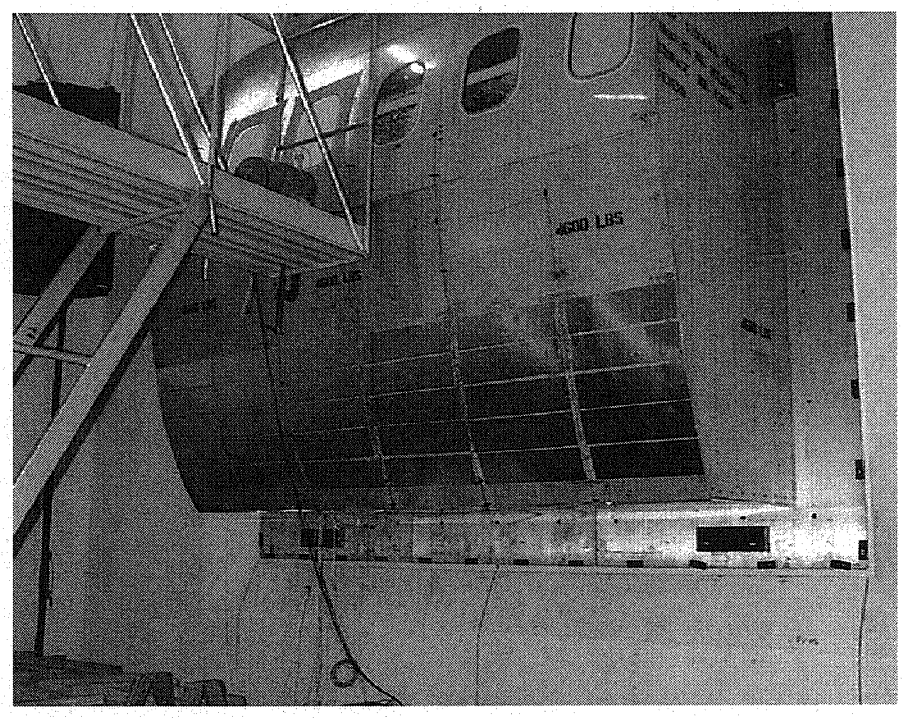

Figure 3.4a. Fuselage sidewall section mounted in the INTF test

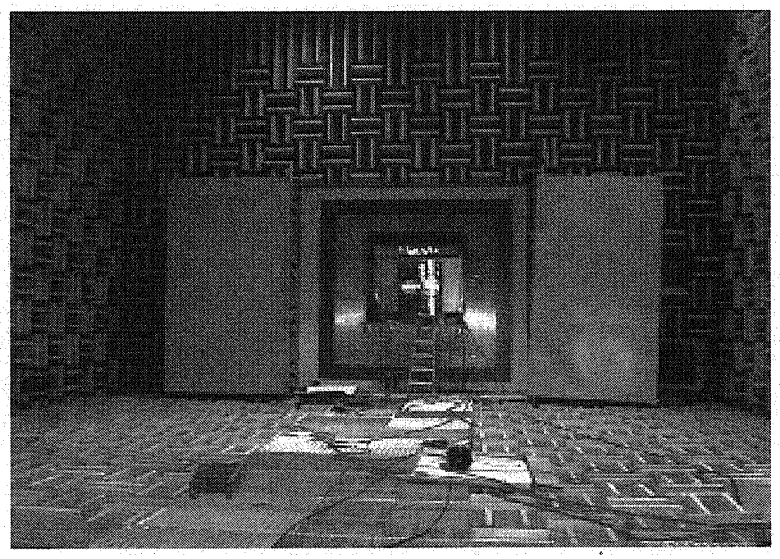

Figure 3.4b. Fuselage sidewall section mounted in the INTF test

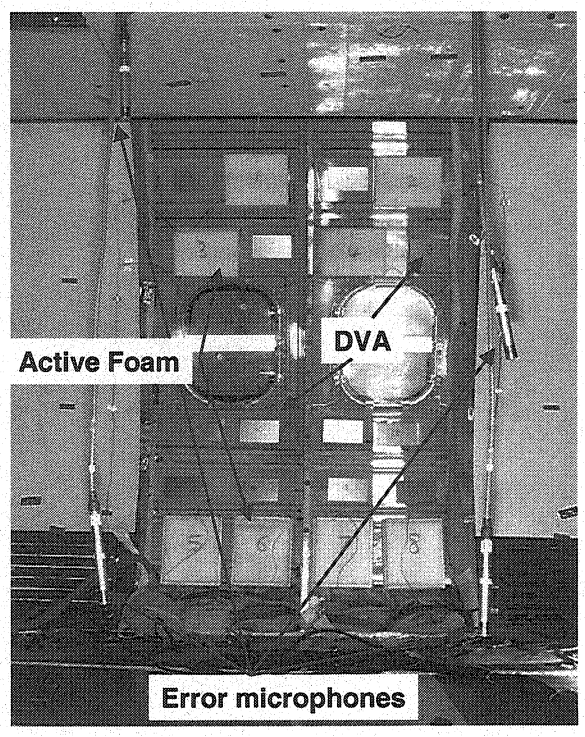

Figure 3.5a. Test panel area and smart foam/DVA test arrangement

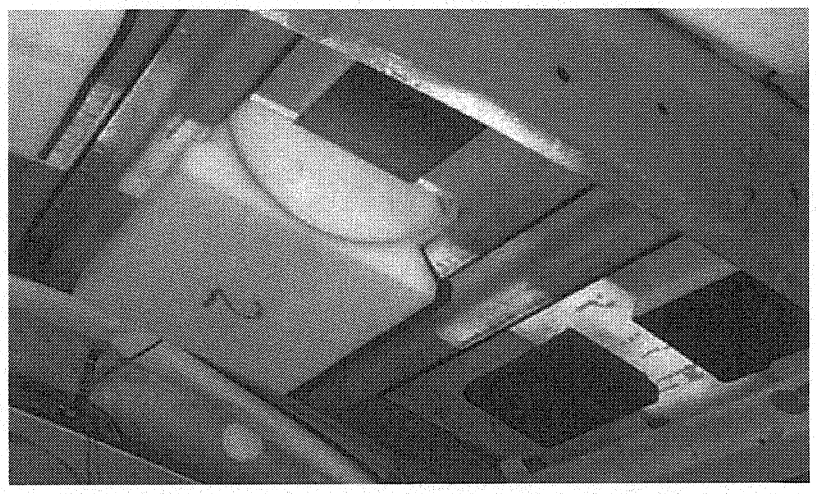

Figure 3.5b. Close up of smart foam and DVA elements

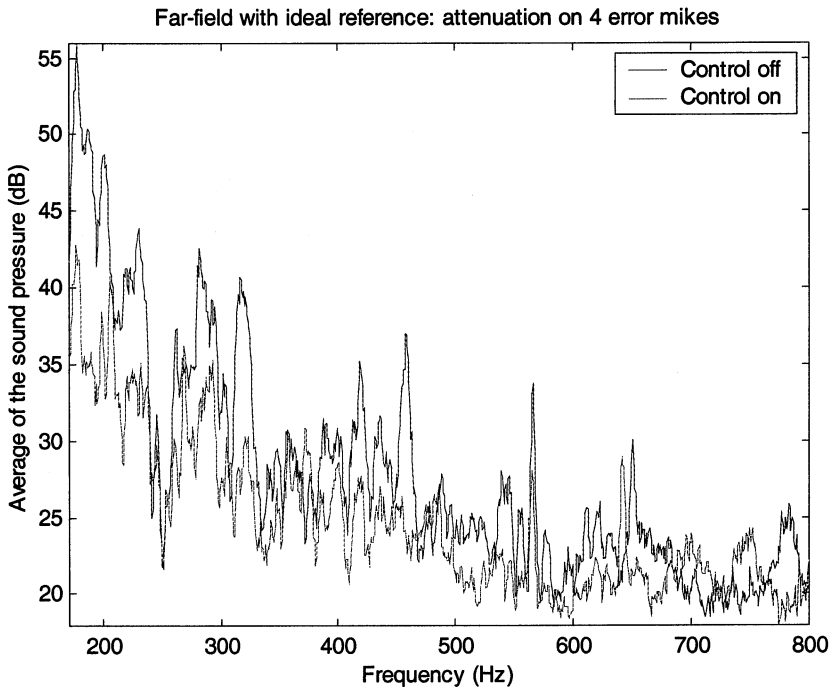

Figure 3.6a. Stiffened panel tests: noise reduction achieved at 4 error sensors with a 4 x 4 x 4 controller and ideal reference.

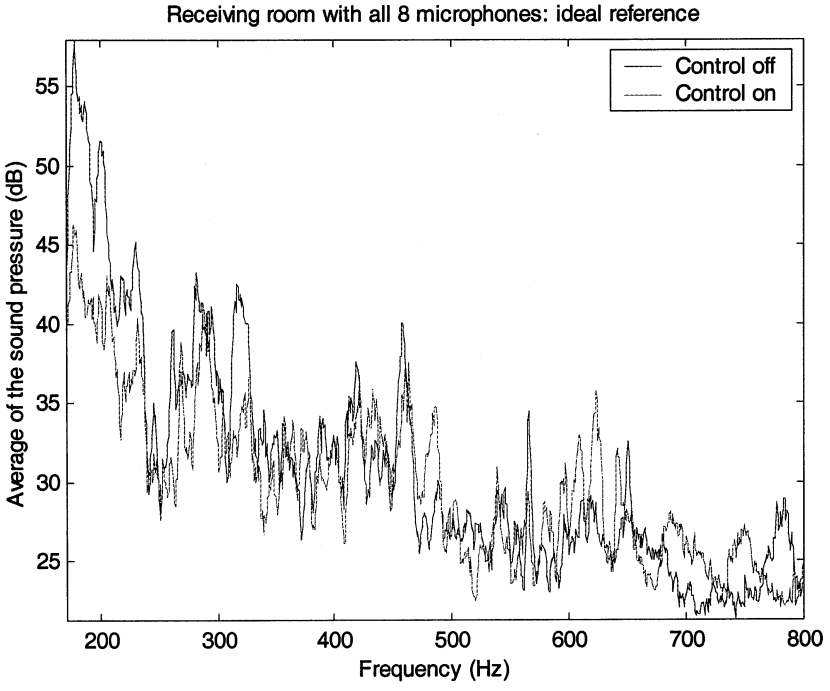

Figure 3.6b. Stiffened panel tests: noise reduction achieved at 8 far-field microphones with a 4 x 4 x 4 controller and ideal

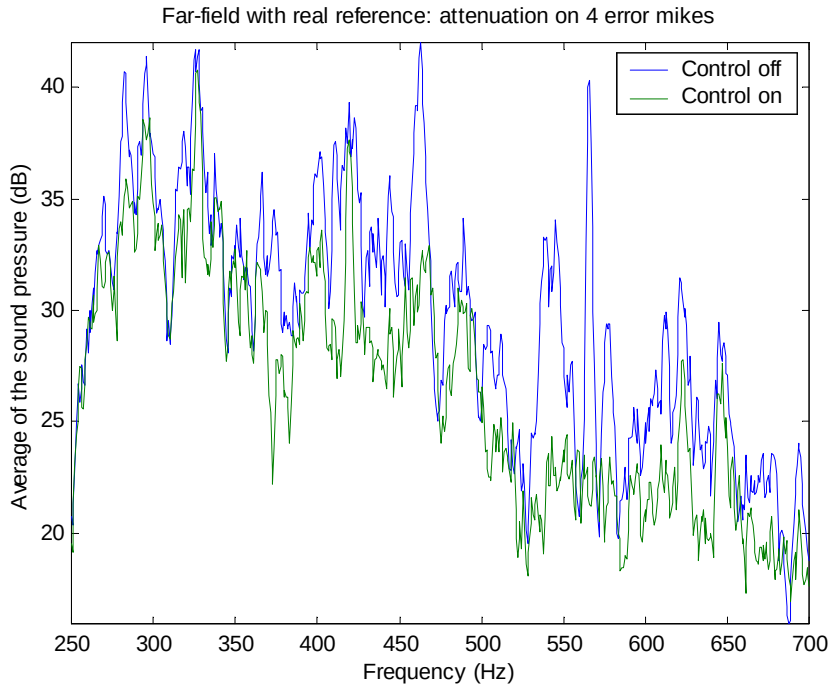

Figure 3.7a. Stiffened panel tests: noise reduction achieved at 4 error sensors with a 4 x 4 x 4 controller and accelerometer reference sensors

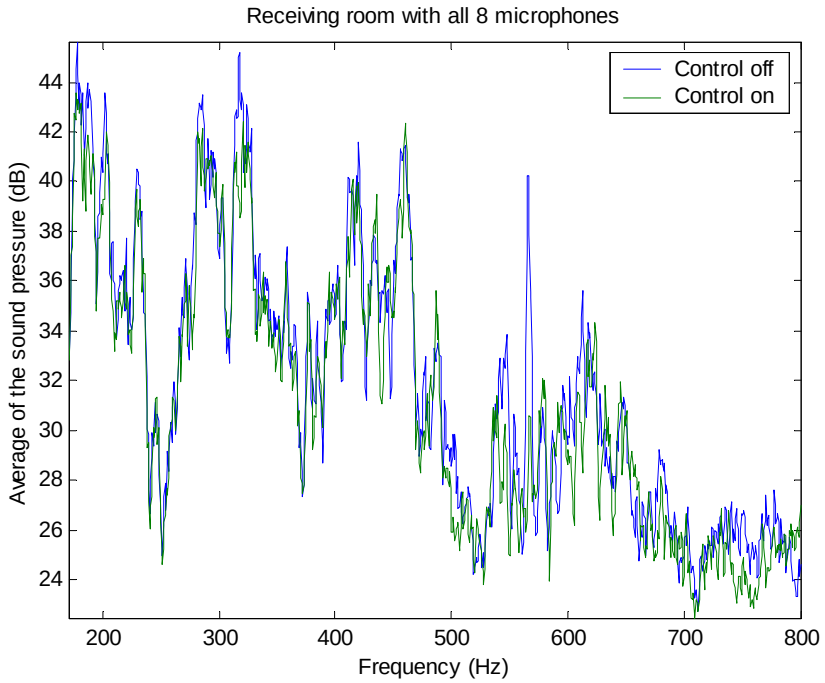

Figure 3.7b. Stiffened panel tests: noise reduction achieved at 8 far-field monitoring microphones with a 4 x 4 x 4 controller and accelerometer reference sensors.

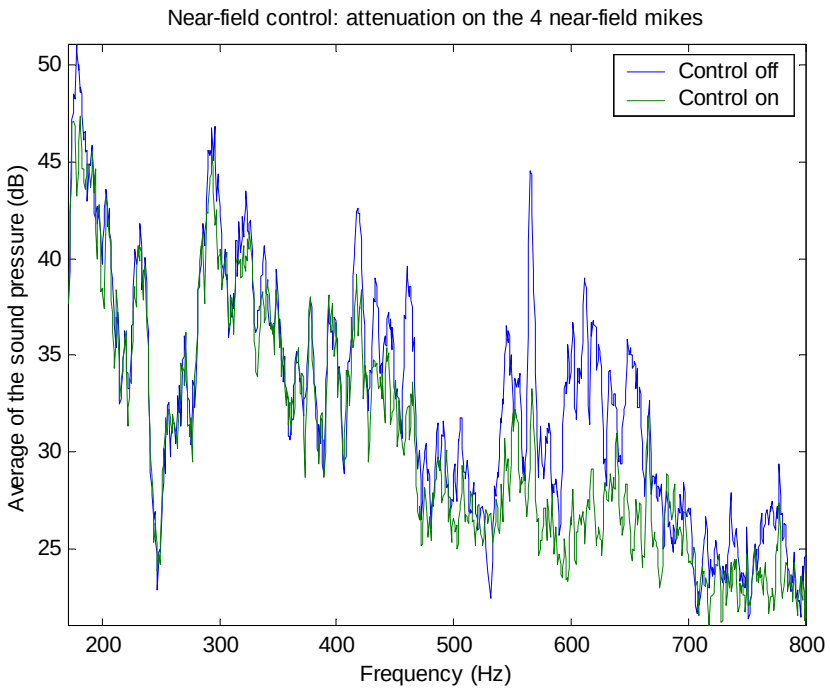

Figure 3.8a. Stiffened panel tests: noise reduction achieved at 4 error microphones with a 4 x 4 x 4 controller and near-field microphone reference sensors.

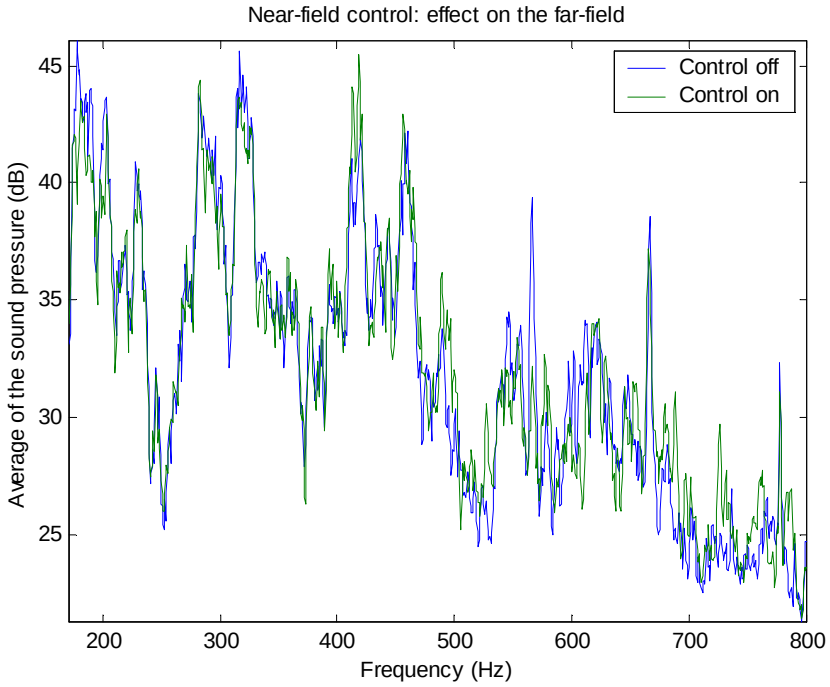

Figure 3.8b. Stiffened panel tests: noise reduction achieved at 8 far-field microphones with a 4 x 4 x 4 controller and near-field microphone reference sensors.

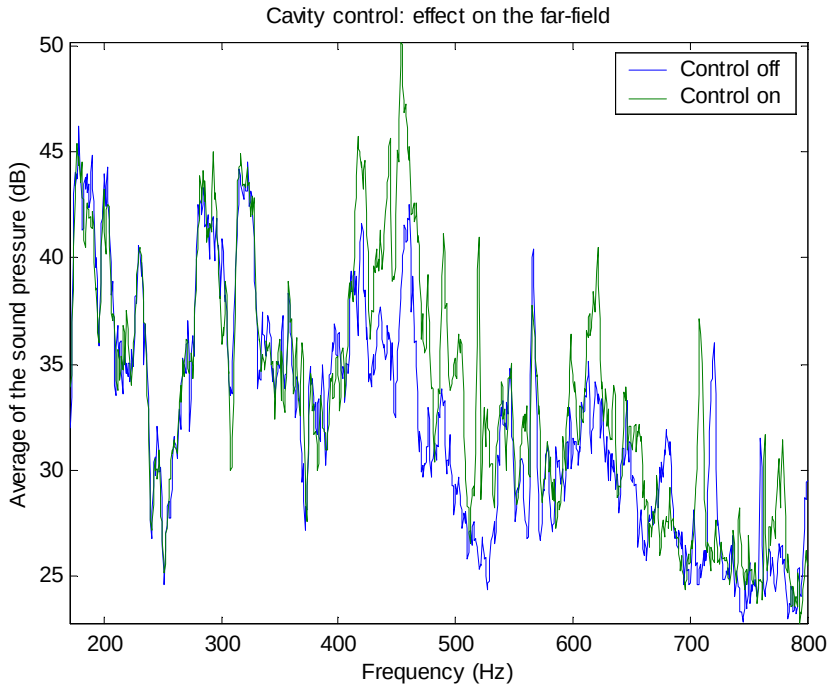

Figure 3.9a. Stiffened panel tests: noise reduction achieved at 4 error sensors with a 4 x 4 x 4 controller and cavity microphones as reference sensors.

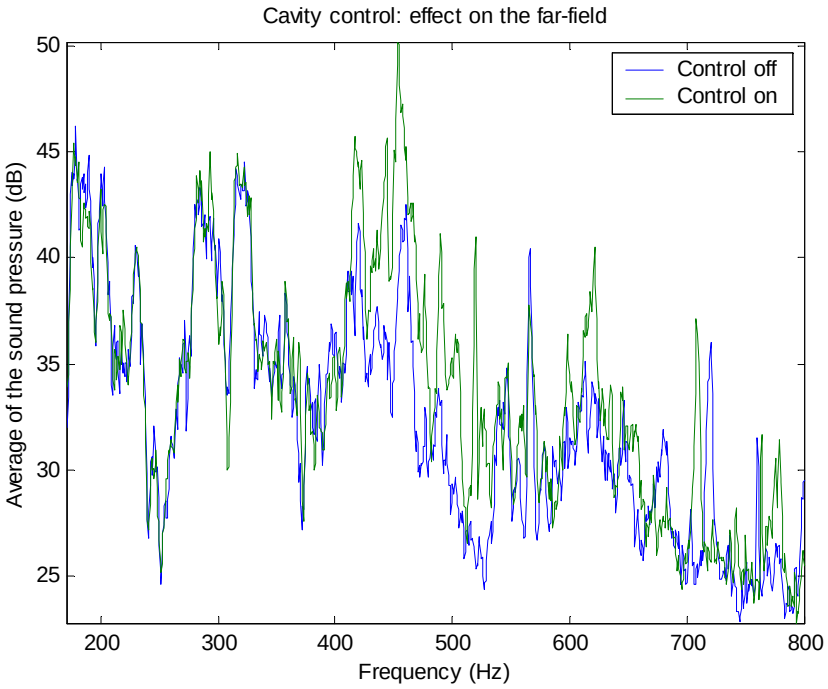

Figure 3.9b. Stiffened panel tests: noise reduction achieved at far-field microphones with a 4 x 4 x 4 controller and cavity microphones as reference sensors.

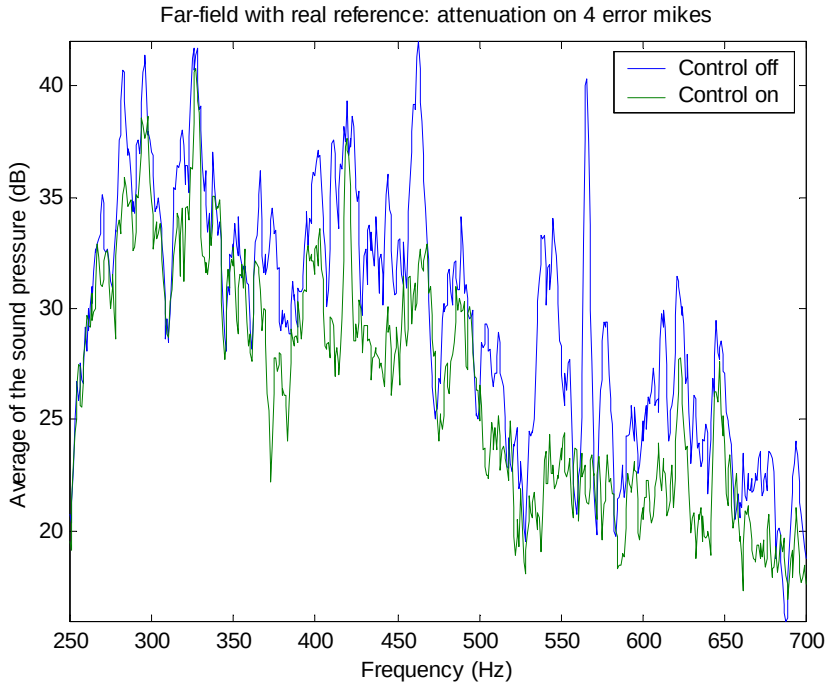

Figure 3.10. Stiffened panel tests: noise reduction achieved at 4 error sensors with a 4 x 4 x 4 controller and accelerometer sensors as reference sensors – reduced control bandwidth.

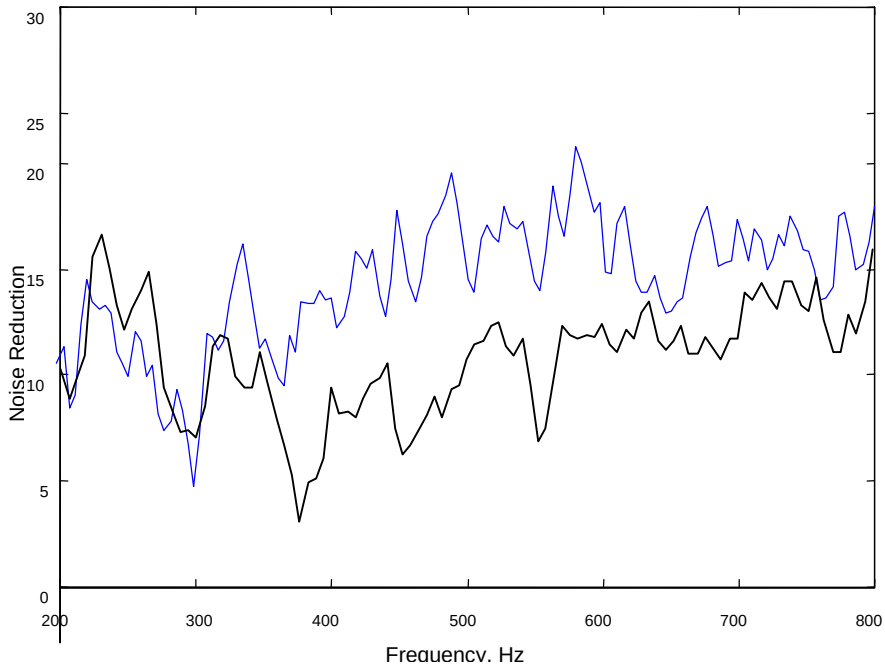

Figure 3.11. Noise Reduction comparison without trim panel in place, acoustic excitation.

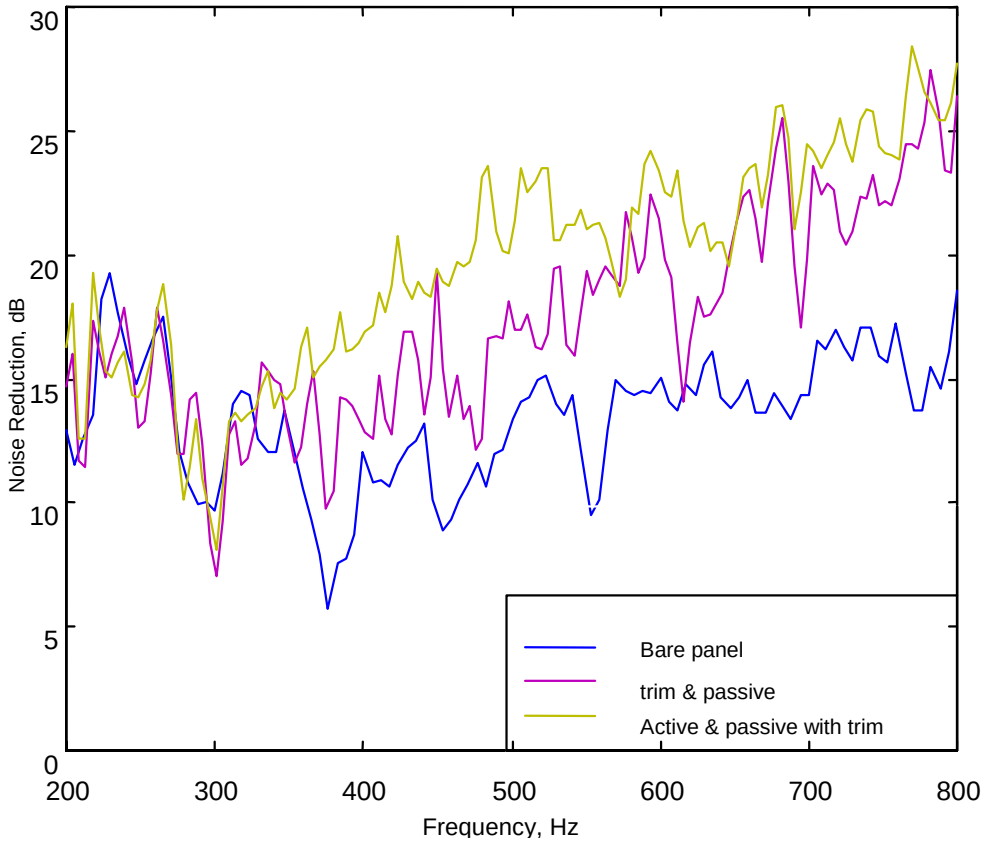

Figure 3.12 Noise Reduction comparison with trim panel in place, acoustic excitation.

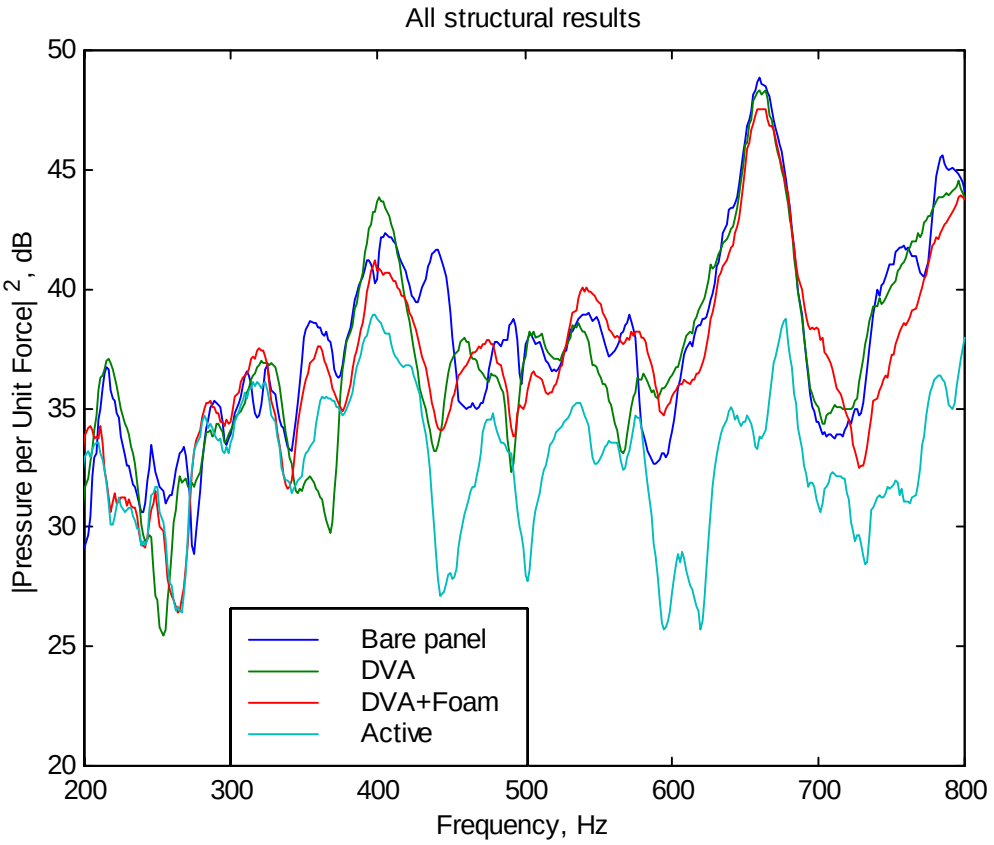

Figure 3.13 Fuselage Transfer Function without trim panel: smart foam and DVA's; with control and without; control shaker excitation.

4. SMART FOAM SYSTEM DESIGN FOR FLIGHT TESTING

The previous work demonstrated the potential of the smart foam and DVA system for providing significant increases in aircraft panel transmission losses in the 300 to 1000 Hz bandwidth in a lightweight, conformal configuration. The tests, however, also established some of the limitations of the present active control arrangement. Although the DSP system used was quite powerful, the controller was limited to a four-reference, four-actuator, four-error sensor system. Thus the area to be treated is limited to four smart foam elements. In practice treating large areas of the aircraft fuselage will require many smart foam elements in a nearly continuous layer. It is not cost effective to keep increasing the DSP power and CPU so that higher order systems could be used. In addition the use of error sensors in the far-field are not practical since they lead to cross-coupling between the active smart foam elements, and installation is difficult. Thus an alternative, more realistic configuration was studied. This system was based upon earlier work performed at Virgina Tech under NASA funding in which multiple de-coupled control elements were used instead of a fully coupled system.

Figure 4.1 shows a schematic arrangement of the uncoupled control system. In this case reference sensors are located under each smart foam element. The reference sensor signal is passed through a single adaptive filter and fed to the smart foam element. A near-field microphone array is located above each smart foam element and used to converge the adaptive filter using a SISO LMS algorithm. In order to decouple the smart foam element from the neighboring noise and control fields, special sensor configurations have to be used. The reference and error sensor arrays consist of a ring of three accelerometers and microphones respectively. This sensor configuration has maximum sensitivity at its center and reduced sensitivity to waves travelling towards the array from outside its sensor circle. The sensor configuration thus allows reduction of noise local to each smart foam element and rejection of non-local information. Each smart foam element thus consists of a reference sensor, a SISO feedforward controller and an error sensor all integrated into a treatment package. Such smart foam elements would then easily be located in the fuselage in a nearly continuous layer of multiple elements. In addition since the controller is SISO, the DSP requirements are very small and a cost-effective electronic unit with

integrated DSP and power electronics could be constructed. Such electronics are presently under construction in the Structural Acoustics Branch at NASA Langley.

A laboratory test was performed on the 757 sidewall in the INTF to validate the above concept. Figure 4.2 shows a picture of two SISO uncoupled smart foam control systems located at the floor level. In this case two smart foam elements are hard-wired together to act as one control actuator. Figure 4.2 shows a close up of one of the SISO smart foam systems. The error sensor array is shown and consists of three microphones located on a circle at three inches above the smart foam surface. The reference sensor consists of three accelerometers located on a circle on the sub-panel under the two smart foam elements (which are wired together as one control channel).

Figure 4.3 shows the performance of the system versus frequency. For comparison the fully coupled LMS control is also shown and achieves about 8dB sound reduction from 300 to 750Hz. The two uncoupled SISO loops achieve nearly similar reductions of about 7dB across 300 to 750 Hz. Thus comparable performance is achieved in a cost-effective and much less complex arrangement with sensors integrated near the smart foam surface.

The results thus validate the proposed flight test system. Work tasks that remain to be done on this concept before the flight test can occur are: (1) develop the SISO DSP and power electronics; (2) program the SISO feedforward adaptive controller; (3) develop practical reference and error sensor arrays; and (4) validate the SISO uncoupled approach over an extended fuselage area with multiple smart foam elements.

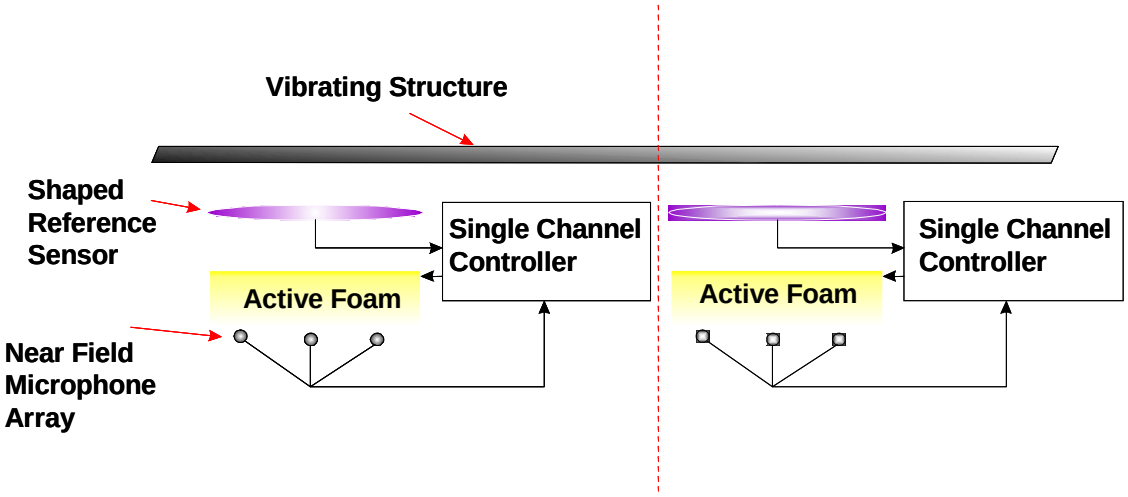

Figure 4.1 Schematic arrangement of uncoupled SISO control approach

Figure 4.2 Two SISO smart foam systems installed in test rig

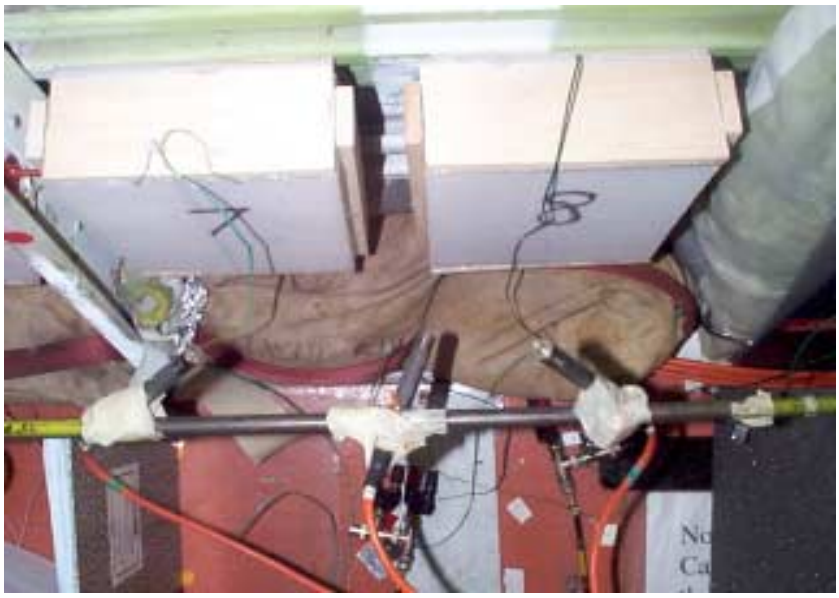

Figure 4.3 Close up of SISO error array.

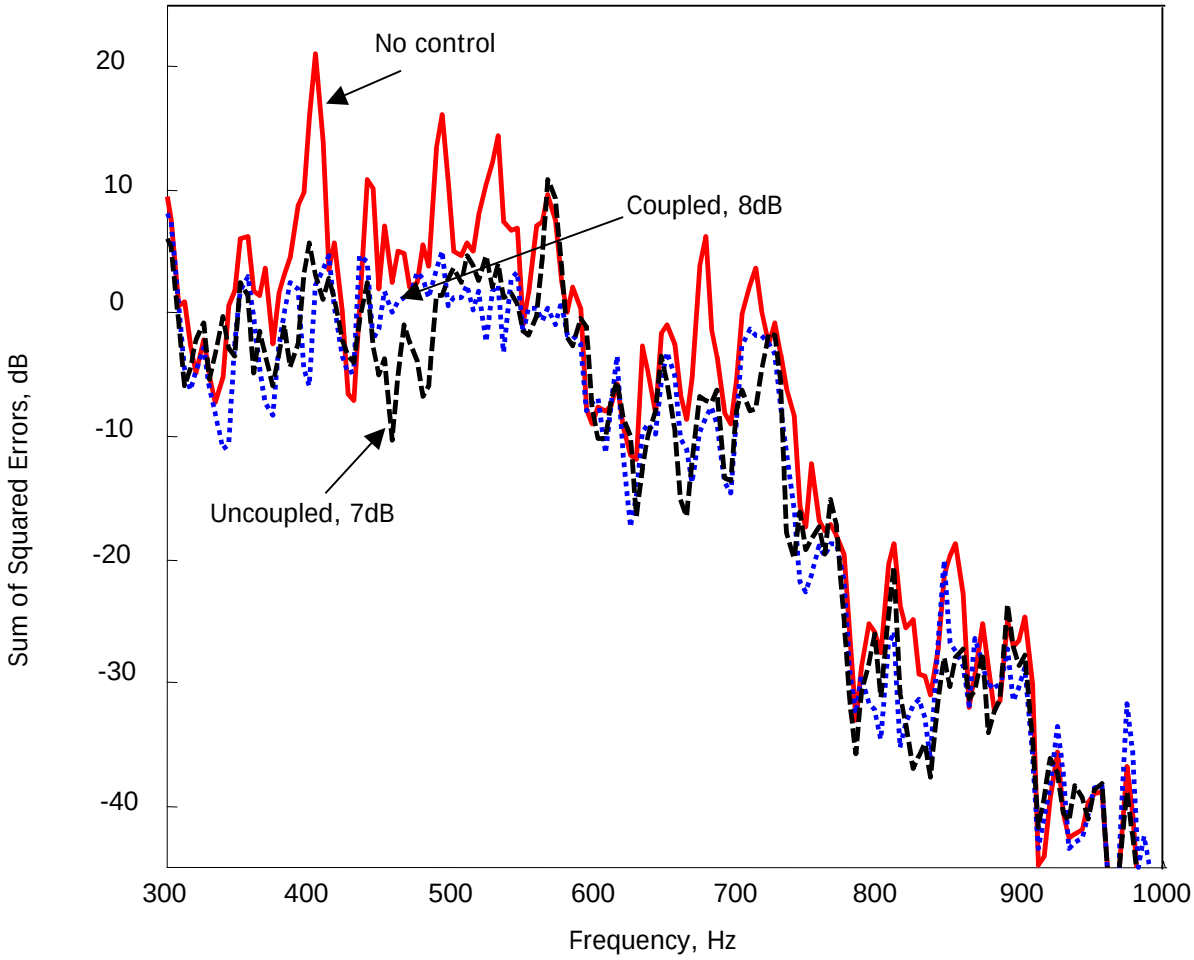

Figure 4.4 Performance comparison of a SISO uncoupled control approach vs a coupled approach.

5. CONCLUSIONS AND RECOMMENDATIONS

This report summarizes the results of investigations conducted by the Boeing Company in 2000-2001 under two subtasks of Task 14, "Structural Acoustic Prediction and Interior Noise Control Technology," of Contract NAS1-97040. One of the subtasks involved development of a finite-element based prediction tool for double-wall panel systems with poro-elastic smart foam and validation of the model with test data, while the other subtask involved experimental evaluations of smart foam treatment for broad band noise control. The following conclusions and recommendations can be made based on the analytical and experimental investigations conducted.

(1) A 3-diemnsional finite element code was developed for modeling a smart foam noise control treatment for an aircraft sidewall section. A step-by-step process was used to build the smart foam finite element code from individual medium elements to multiple coupled interface matrices, along with the corresponding intermediate validations. The FE code can be used to predict surface impedance of the poro-elastic foam, cavity pressures and structural responses, to determine sound absorption coefficients of multiple media coupled systems, and to calculate sound transmission loss of a double-panel with different foam-lined configurations.

(2) Extensive laboratory tests were conducted on several configurations of passive and active smart foam actuators attached to a stiffened flat panel and a stiffened 757-sidewall section. The following conclusions may be drawn from these tests: (i) significant improvement in noise reduction of the test panel and the fuselage section were observed for both acoustic and structural excitations due to active control with smart foam actuators, (ii) accelerometers on the source plate provide very good references for the controller, (iii) the 4 x 4 x 4 controller configuration was effective for achieving significant reductions at error sensors, (iv) control strategies using far-field microphones as error sensors lead to very good broadband attenuation, but more error sensors/actuators would be needed to control the sound pressure over the entire receiving room at high frequencies, (v) good attenuation at near-field microphones allows some attenuation at far-field microphones, (vi) strategies using error microphones in cavities and accelerometers as volume velocity sensors are not working well on the far-field attenuation at the present time; further investigation are needed for those cases.

(3) Based on the good noise reductions obtained with the smart foam actuator configuration used in the 757-sidewall tests, it is recommended that a similar smart foam configuration be used in upcoming 757 flight tests. However, the overall system design can be improved by adopting an uncoupled approach using multiple SISO smart foam systems instead of the 4x4x4 coupled smart foam system used in the lab tests. Further development and validation of the system electronics, controller algorithms, and sensor arrays is recommended before this smart foam treatment package is installed on the 757 aircraft.

6.0 REFERENCES

[1] “Control of aircraft interior broadband noise with foam-PVDF smart skin,” C. Guigou and C. R. Fuller, Journal of Sound and Vibration, 220(3), pp. 541-557, 1999

[2] “Control of the noise radiated by a plate using a distributed active vibration absorber (DAVA),” P. Marcotte, C. R. Fuller and P. Cambou, Proceedings of Active 99, Fort Lauderdale, FL, USA,1999

[3] “A study of smart foam for noise control applications,” Cassandra A. Gentry-Grace, Ph.D. thesis, Mechanical Engineering Dept., Virginia Polytechnic Institute & State University, 1998

[4] “The theory of propagation of elastic waves in a fluid-saturated porous solid. I Low frequency range,” M. A. Biot, J. Acoust. Soc. Am. 28, 168-191, 1956

[5] “An efficient finite element scheme for solving the three-dimensional poroelasticity problem in acoustics,” R. Panneton and N. Atalla, J. Acoust. Soc. Am. 101 (6), 3287-3298, 1997

[6] “A finite element method for determining the acoustic modes of irregular shaped cavity,” M. Petyt, Journal of Sound and Vibration, 45(4), pp. 495-502, 1976

[7] “Introduction to finite element vibration analysis,” Maurice Petyt, Cambridge

University Pres, 1990

[8] “Finite element modeling of isotropic elastic porous materials coupled with acoustical finite elements,” Y. J. Kang and J. S. Bolton, J. Acoust. Soc. Am. 98 (1), 635-643, 1995

[9] “Numerical prediction of sound transmission through finite multilayer systems with poroelastic materials,” R. Panneton and N. Atalla, J. Acoust. Soc. Am. 100 (1), 346-354, 1996

[10] “Propagation of sound in porous media: Modelling sound absorbing materials,” Elsevier, New York, 1993

[11] “Smart Foam for Active Control of Sound,” Bolton, J. S. and Green, E. R., Second Conference on Recent Advances in Active Control of Sound and Vibration, Blacksburg, VA, 139-149, 1993

[12] “Control of Sound Radiation/Reflection with Adaptive Foams,” Fuller, C. R., Bronzel, M. J., Gentry, C. A. and Whitington, D. E., Proc. Noise-Con 94, May 1994.

[13] “Smart Foam for Applications in Passive/Active Noise Reduction Control,” Gentry, C. A., Guigou, C and Fuller, C. R., Journal Acoust. Soc. Am., 10(4), 1771-1778, 1997.

[14] “Smart Foam Lines Trim Panels for Aircraft Cabin Noise Control,” Mathur, G. P., Fuller, C. R., Johnson, M. E., and D’Angelo, J, Paper presented at the 6th AIAA/CEAS Aeroacoustics Conference, Lahaina, Hawaii, 12 – 1, 4 June 2000.

Appendix A

1. Stiffness and mass matrices for poroelastic element

$$[M_{ss}] = \sum \int [N_u]^{e^T} \rho_{11} [N_u]^e dV$$

$$[M_{sf}] = \sum \int [N_u]^{e^T} \rho_{12} [N_U]^e dV$$

$$[M_{ff}] = \sum \int [N_U]^{e^T} \rho_{22} [N_U]^e dV$$

$$[K_{ss}] = \sum \int [B_u]^{e^T} [D_s] [B_U]^e dV$$

$$[K_{sf}(\omega)] = \sum \int [B_u]^{e^T} [D_{sf}(\omega)] [B_U]^e dV$$

$$[K_{ff}(\omega)] = \sum \int [B_U]^{e^T} [D_f(\omega)] [B_U]^e dV$$

$$[C_{ss}] = \sum \int [N_u]^{e^T} b(\omega) [B_u]^e dV$$

$$[C_{sf}] = \sum \int [N_u]^{e^T} b(\omega) [B_U]^e dV$$

$$[C_{ff}] = \sum \int [N_U]^{e^T} b(\omega) [B_U]^e dV$$

$$[F_s] = \sum \int [N_u]^{e^T} (\{f\} - h\{f_n\}) dS$$

$$[F_f] = \sum \int [N_U]^{e^T} h\{f_n\}) dS$$

where $[B_u]^e = [L][N_u]^e$ and $[B_U]^e = [L][N_U]^e$

2, Stiffness and mass matrices for acoustic element

$$[K_a] = \sum \int [B_a]^{e^T} [B_a]^e dV$$

$$[B_a] = \begin{bmatrix} \frac{\partial}{\partial x} \\ \frac{\partial}{\partial y} \\ \frac{\partial}{\partial z} \end{bmatrix} \lfloor N_a \rfloor_i$$

$$[M_a] = \sum \int [N_a]^{e^T} [N_a]^e dV$$

REPORT DOCUMENTATION PAGE

Form Approved
OMB No. 0704-0188

1. AGENCY USE ONLY (*Leave blank*)	2. REPORT DATE	3. REPORT TYPE AND DATES COVERED
	November 2001	Contractor Report

4. TITLE AND SUBTITLE
Structural Acoustic Prediction and Interior Noise Control Technology

5. FUNDING NUMBERS
C NAS1-97040
TA 14
WU 706-81-14-01

6. AUTHOR(S)
G. P. Mathur, C. L. Chin, M. A. Simpson, and J. T. Lee

7. PERFORMING ORGANIZATION NAME(S) AND ADDRESS(ES)
The Boeing Company
Long Beach, CA 90807

8. PERFORMING ORGANIZATION REPORT NUMBER

9. SPONSORING/MONITORING AGENCY NAME(S) AND ADDRESS(ES)
National Aeronautics and Space Administration
Langley Research Center
Hampton, VA 23681-2199

10. SPONSORING/MONITORING AGENCY REPORT NUMBER
NASA/CR-2001-211247

11. SUPPLEMENTARY NOTES
Langley Technical Monitor: Daniel L. Palumbo

12a. DISTRIBUTION/AVAILABILITY STATEMENT
Unclassified-Unlimited
Subject Category 71 Distribution: Nonstandard
Availability: NASA CASI (301) 621-0390

12b. DISTRIBUTION CODE

13. ABSTRACT (*Maximum 200 words*)

This report documents the results of Task 14, "Structural Acoustic Prediction and Interior Noise Control Technology" of Contract NAS1-97040 with The Boeing Company. The task was to evaluate the performance of tuned foam elements (termed Smart Foam) both analytically and experimentally. Results taken from a three-dimensional finite element model of an active, tuned foam element are presented. Measurements of sound absorption and sound transmission loss were taken using the model. These results agree well with published data. Experimental performance data were taken in Boeing's Interior Noise Test Facility where 12 smart foam elements were applied to a 757 sidewall. Several configurations were tested. Noise reductions of 5-10 dB were achieved over the 200-800 Hz bandwidth of the controller. Accelerometers mounted on the panel provided a good reference for the controller. Configurations with far-field error microphones outperformed near-field cases.

14. SUBJECT TERMS
Aircraft Interior Noise; Active/Passive Noise Control; Smart Foam; Finite Element Model

15. NUMBER OF PAGES
70

16. PRICE CODE
A04

17. SECURITY CLASSIFICATION OF REPORT	18. SECURITY CLASSIFICATION OF THIS PAGE	19. SECURITY CLASSIFICATION OF ABSTRACT	20. LIMITATION OF ABSTRACT
Unclassified	Unclassified	Unclassified	UL